Review and syntheses: Ocean alkalinity enhancement and carbon dioxide removal through marine enhanced rock weathering using olivine

Luna J. J. Geerts[1], Astrid Hylén[1], Filip J. R. Meysman[1,2]

[1]Geobiology, Department of Biology, University of Antwerp, 2610 Wilrijk Antwerp, Belgium
[2]Department of Biotechnology, Delft University of Technology, Van der Maasweg 9, 2629 HZ Delft, The Netherlands

Correspondence: Luna J. J. Geerts (luna.geerts@uantwerpen.be)

Abstract. Marine enhanced rock weathering (mERW) is increasingly receiving attention as a marine-based carbon dioxide removal (CDR) technology. The method aims to achieve ocean alkalinity enhancement (OAE) by introducing fast-weathering rocks into coastal systems. The latter is envisioned to act as a large natural biogeochemical reactor, where ambient physical and biological processes can stimulate rock dissolution, thus generating a concomitant alkalinity release and increasing the seawater's capacity to sequester CO_2. Olivine has been forwarded as the prime candidate mineral for mERW, but to the present, no results are available from larger scale field studies in coastal areas, so the information about olivine dissolution in marine systems is largely derived from laboratory experiments. As a result, key uncertainties remain concerning the efficiency, CO_2 sequestration potential, and impact of olivine-based mERW under relevant field conditions. In this review, we summarize recent research advancements to bridge the gap between existing laboratory results and the real-world environment in which mERW is intended to take place. To this end, we identify the key parameters that govern the dissolution kinetics of olivine in coastal sediments, and the associated CO_2 sequestration potential, which enable us to identify a number of uncertainties that are outstanding with respect to the implementation and upscaling of olivine-based ERW, as well as the monitoring, reporting, and verification (MRV). From our analysis, we conclude that the current knowledge base is not sufficient to predict the outcome of *in situ* mERW applications. Particularly, the impact of pore water saturation on the olivine dissolution rate and the question of the additionality of alkalinity generation remain critical unknowns. To more confidently assess the potential and impact of olivine-based mERW, dedicated pilot studies under field conditions are needed, which should be conducted at a sufficiently large spatial scale and monitored for a long enough time with sufficient temporal resolution. Additionally, our analysis indicates that the specific sediment type of the application site (e.g. cohesive versus permeable) will be a critical factor for olivine-based mERW applications, as it will significantly impact the dissolution rate by influencing the ambient pore water pH, saturation dynamics, and natural alkalinity generation. Therefore, future field studies should also target different coastal sediment types.

1 Introduction

1.1 Carbon dioxide removal through ocean alkalinity enhancement

Climate stabilization is a pressing challenge for society (IPCC, 2023). Scenario analysis reveals that in addition to decarbonization, active removal of carbon dioxide (CO_2) from the atmosphere will be required to reach the targets of the COP21 Paris agreement (IPCC, 2023; Sanderson et al., 2016; UNFCCC, 2015). Such carbon dioxide removal (CDR) has to happen fast and at a sufficiently large scale: gigaton (Gt) capacity must be reached already by 2040 and this effort should increase to 12–15 Gt CO_2 yr^{-1} by 2100 (Rockström et al., 2017; Minx et al. 2018). As such, the need for technologies that can deliver such gigaton-scale CDR is high. However, research on the topic is currently still at an early stage, and so the efficiency, reliability, and environmental impact of most CDR techniques remain poorly constrained (Fuss et al., 2018; Minx et al., 2018; NASEM, 2022; Smith et al., 2016; Terlouw et al., 2021).

One proposed CDR technique is ocean alkalinity enhancement (OAE), which aims to increase the ocean's capacity to store CO_2 by raising the alkalinity level of surface waters (Hartmann et al., 2013; Renforth and Henderson, 2017). Alkalinity is the excess of proton acceptors (bases) over proton donors (acids) in solution and governs the CO_2 storage capacity of seawater (Dickson, 1984; Zeebe and Wolf-Gladrow, 2001). The addition of alkalinity shifts the reaction equilibria of the carbonate system from dissolved CO_2 towards bicarbonate (HCO_3^-) and carbonate (CO_3^{2-}), thus allowing more atmospheric CO_2 to dissolve in the seawater (Fig. 1) (Wolf-Gladrow et al., 2007). Alkalinity production through the weathering of silicate minerals and subsequent drawdown of atmospheric CO_2 is the feedback that regulates Earth's climate on geological timescales (Berner, 2004; Berner et al., 1983), and natural silicate weathering will eventually neutralize the CO_2 currently being released from anthropogenic activities (Archer et al., 2009). However, the timescale of this response is too slow (> 10,000 years) for society. Even if emissions were completely halted, we would have to "sit through" an extended period of global warming before the excess of anthropogenic CO_2 is removed naturally (Archer et al., 2009). Therefore, OAE aims to mimic the natural way by which the Earth system has responded in the geological past, but at an elevated pace. This nature-based character of OAE could help increase the societal acceptance of the CDR method (Corner and Pidgeon, 2015). Compared to other CDR approaches, OAE has the advantage that the CO_2 sequestration potential is considered to be substantial (>0.1–1 Gt CO_2 yr^{-1}) and that CO_2 storage is essentially permanent over a time scale of thousands of years (Archer et al., 2009; Caserini et al., 2021, 2022; NASEM, 2022; Renforth and Henderson, 2017). Moreover, OAE has the important benefit of counteracting ocean acidification, which is not the case for other CDR techniques that only target CO_2 sinking, such as reforestation on land, or blue carbon and ocean fertilization in the marine environment (Campbell et al., 2022; Caserini et al., 2022; Meysman and Montserrat, 2017).

The crux of any OAE technique relates to the source of the alkalinity, and several different OAE approaches have been suggested (NASEM, 2022). "Fast-addition OAE approaches" aim to introduce alkalinity directly to surface waters, and the alkalinity is generated either by electrochemical methods (generation of base, such as NaOH, through electrolysis of seawater) or by ocean liming (addition of nearly instantly dissolving basic minerals, such as $Ca(OH)_2$ or $Mg(OH)_2$) (Campbell et al.,

2022; Caserini et al., 2022; Eisaman et al., 2023; Rau et al., 2018; Renforth and Henderson, 2017) (Fig. 1). These technologically-oriented methods require the construction of large reactor infrastructure to produce the alkaline products that enable OAE (electrolyzer plants, lime kilns), thus necessitating substantial capital investments (NASEM, 2022; Rau, 2008;

65 Renforth et al., 2013). These approaches also need high amounts of energy per ton of CO_2 sequestered (electrochemistry) or require the installation of additional carbon capture capacity (CO_2 capture during lime production). In contrast, "slow-addition OAE approaches" are based on chemical mineral weathering, and are "nature-inspired" in the sense that they aim to mimic a natural process of alkalinity generation.

The idea underlying marine enhanced rock weathering (mERW) is to add specific mineral types to coastal and shelf sediments,

70 which then gradually dissolve over a time scale of years to centuries, thus gradually releasing alkalinity from the seabed to the overlying water (Campbell et al., 2022; Hartmann et al., 2013; NASEM, 2022). The production of rapidly weathering minerals and their addition to the seafloor requires far less energy than technology-oriented approaches, as it capitalizes on natural energy sources, such as the exergonic nature of the dissolution reaction and the *in situ* "milling" of particles using energy from waves and currents (Meysman and Montserrat, 2017; NASEM, 2022). Moreover, no large reactor infrastructure is needed, as

75 one essentially uses the coastal system as the biogeochemical reactor. As such, the method offers the prospect of rapid scalability, as it can be integrated within current marine engineering practices (e.g. beach nourishment, dredging, land reclamation) using existing technology and infrastructure (ports, ships, dredging equipment) (Meysman and Montserrat, 2017). A range of minerals have been considered as source material for mERW, including naturally occurring silicates (Bach et al., 2019; Hartmann et al., 2013; Lackner, 2002; NASEM, 2022; Renforth and Henderson, 2017) and carbonates (Harvey, 2008),

80 but also waste and overburden material (Bullock et al., 2021; Renforth, 2019; Vandeginste et al., 2024). Nevertheless, the most attention has so far been devoted to the silicate mineral olivine (Feng et al., 2017; Flipkens et al., 2023b; Fuhr et al., 2022, 2023, 2024; Griffioen, 2017; Hangx and Spiers, 2009; Hauck et al., 2016; Köhler et al., 2013; Li et al., 2024; Meysman and Montserrat, 2017; Montserrat et al., 2017; Rigopoulos et al., 2018), which is characterized by a fast intrinsic weathering rate, high CO_2 uptake, and large relative abundance. In this review, we synthesize the current knowledge on mERW using olivine

85 as a way to achieve OAE.
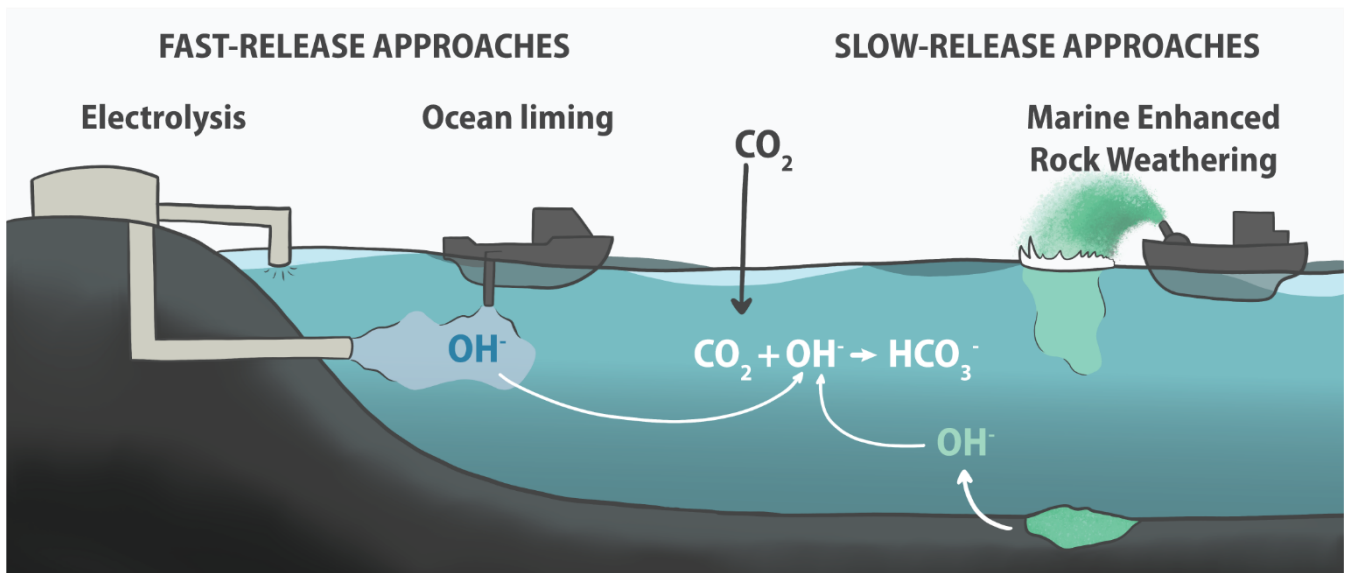
Figure 1. Ocean alkalinity enhancement. During fast-release approaches (left), alkalinity is directly introduced into the ocean by electrolysis of seawater (which creates NaOH) or through ocean liming (addition of nearly instantly dissolving basic minerals, such as $Ca(OH)_2$ or $Mg(OH)_2$). During slow-release approaches (right), minerals (e.g., olivine) are applied to the seafloor, and alkalinity is slowly released via chemical weathering.

1.2 Ocean alkalinity enhancement via enhanced rock weathering

The ultimate aim of mERW is to accelerate rock weathering, reducing the timescale of the resulting CO_2 uptake from millennia down to decennia. This enhanced weathering can be achieved by selectively using source rocks or minerals that have high dissolution rates, pulverizing the source rock into small particles to increase the reactive surface area, and distributing the particles in areas with high weathering potential (Meysman and Montserrat, 2017). During mERW, minerals can dissolve in the water column or be applied to the sediment. In effect, most modelling targeting the global sequestration potential have focused on rock weathering in the water column. Yet, a large energy investment is required for water column application, as particles must be ground to sufficiently small sizes (~1 µm) to stay in suspension (Köhler et al., 2013), which reduces the CO_2 removal efficiency significantly (up to 30%) when using fossil fuels (Hangx and Spiers, 2009; Köhler et al., 2013). Consequently, most experiments on marine mERW has targeted sediment application (Flipkens et al., 2023b; Fuhr et al., 2022, 2023, 2024; Montserrat et al., 2017; Rigopoulos et al., 2018).

A wide range of minerals has been considered for mERW. The silicate mineral olivine ($Mg_{(2-x)}Fe_xSiO_4$), particularly its Mg-rich end member forsterite, has so far received the most attention in this context due to its rapid intrinsic weathering rate (Table 1), efficient mass-to-mass CO_2 uptake (1.25 g CO_2 g fosterite^{-1}), and high abundance. The silicate minerals wollastonite ($CaSiO_3$; Lackner, 2002; Renforth and Henderson, 2017) and anorthite ($CaAl_2Si_2O_8$; te Pas et al., 2023) have dissolution rates that are comparable to or even higher than forsterite (Table 1). Yet, these minerals have received little attention in the context of mERW, as they are less abundant than olivine and have lower CO_2 capture potentials than forsterite (0.76 g CO_2 g wollastonite^{-1} and 0.32 g CO_2 g anorthite^{-1}, te Pas et al., 2023). Carbonates (calcium carbonate: $CaCO_3$, dolomite: $CaMg(CO_3)_2$)

and brucite ($Mg(OH)_2$) dissolve faster than olivine (the nearly instantaneous dissolution of brucite could put it in the "fast-addition" OAE category; Table 1) and do not contain potentially harmful trace metals (unlike olivine, section 2.1), making them interesting minerals for mERW. However, both carbonates and brucite bear the risk of pore water oversaturation and reprecipitation, thus strongly reducing the CO_2 sequestration efficiency (Bach, 2024; Hartmann et al., 2013, 2022). There has been a recent interest in using brucite as a mineral for OAE via liming (e.g. Hartmann et al., 2022; Yang et al., 2023), but the cost per ton of mineral has been identified as a potential bottleneck (Kramer, 2006; Simandl et al., 2007). Rocks consisting of a multitude of minerals could also be considered for mERW. In the context of terrestrial ERW, basalt application has received considerable attention (Beerling et al., 2018), but the CO_2 capture potential of basalt is significantly lower than that of olivine (Rigopoulos et al., 2018). Recently, there has also been interest in using waste material, such as steel slags and mining side streams, for mERW (Bullock et al., 2021; Moras et al., 2024; Renforth, 2019). Their applicability is still under investigation, but the advantage of these materials is that they are already mined, thereby reducing the overall cost for mERW (Renforth, 2019). However, there are concerns about environmental impacts due to trace metal release from waste minerals (Bullock et al., 2021), although the first results indicate that this effect could be limited (Moras et al., 2024).

Table 1. Dissolution times of different minerals, assuming a 1 mm radius sphere dissolving in water at pH 5 and a temperature of 25°C. Adapted from Lasaga et al. (1994) and Hartmann et al. (2013). [a]The molar volume of albite is greater than that of serpentine, giving the minerals different dissolution times for the same reactivity. The rates reported here were measured in freshwater under well-mixed conditions; in seawater and sediments, the dissolution rate may be lower due to saturation effects.

Mineral	Reactivity (log mol m^{-2} s^{-1})	Dissolution time (years)
Quartz[1]	-13.39	34,000,000
Kaolinite[1]	-13.28	6,000,000
Muscovite[1]	-13.07	2,600,000
Epidote[1]	-12.61	923,000
Albite[a, 1]	-12.26	575,000
Serpentine[a, 2]	-12.26	533,000
Sepiolite[3]	-11.85	79,000
Enstatite[1]	-10.00	10,100
Diopside[1]	-10.15	6,800
Forsterite[4]	**-9.36**	**1680**
Anorthite[1]	-8.55	112
Wollastonite [1]	-8.00	79
Brucite[5]	-7.30	26
Dolomite[6]	-6.70	1.6
Calcite[6]	-5.48	0.1

[1](Lasaga et al., 1994), [2](Orlando et al., 2011), [3](Mulders et al., 2018), [4](Rimstidt et al., 2012), [5](Pokrovsky and Schott, 2004), [6](White and Brantley, 1995)

1.3 Marine enhanced rock weathering in different coastal environments

130   When mineral particles are deposited onto the sediment, they become subjected to a suite of physical, chemical, and biological processes that can stimulate their dissolution, collectively referred to as the "benthic weathering engine" (Meysman and Montserrat, 2017). This biogeochemical "engine" is primarily regulated by the hydrodynamic energy regime at a specific site, as hydrodynamics drives the transport and sorting of particles, controls the sediment transport regime, which includes physical transport processes (advection, diffusion), and key biological transport processes (biomixing, bioirrigation). While coastal

135   sediments represent a range of biogeochemical conditions, biogeochemical fluxes, and rates strongly correlate with the sediment type and the associated dominant transport mechanism (Aller, 2014; Silburn et al., 2017). In highly energetic systems, finer particles are transported away by erosion and deposition cycles or sorted downwards, resulting in gravel beds exposed to bedload transport. The solute transport is dominated by intense advective flushing, which gives the porewater a chemical composition similar to that of the overlying water (Aller, 2014; Huettel and Rusch, 2000; Silburn et al., 2017). When moving

140   to less energetic systems, smaller particles (including some organic matter) remain in place and the sediment consists mostly of sand. The sediment is permeable and advective flow is the primary solute transport mechanism, yet the smaller grain size restricts the water exchange enough to give the pore water a chemical composition that is distinct from the overlying water (Silburn et al., 2017; Widdicombe et al., 2011). In some cases, the advective water exchange can be supplemented by bioirrigation (Kristensen, 2001; Volkenborn et al., 2007). In systems with low hydrodynamic energy, fine particles settle and

145   form cohesive sediments rich in organic matter. The solute exchange in these sediments is driven by diffusion but is dominated by bioirrigation when larger benthic animals are present (Kristensen, 2001).

To identify the dominant controls on mERW, an abstraction into three sediment types is valuable, each with its own specific transport regime, as done in sediment transport modelling studies (e.g., Le Hir et al., 2011; Ouillon, 2018). In the *bedload scenario* (Fig. 2b), silicate sand is deposited in areas with high hydrodynamic energy and large grain sizes to promote further

150   physical grinding of the silicate grains during bedload transport (Meysman and Montserrat, 2017). In this scenario, minerals remain in close contact with the overlying seawater, and the weathering primarily takes place on top of the seafloor. In the *permeable sediment scenario* (Fig. 2c), silicate sand is mixed into permeable sand sediments. The advective flushing prevents the build-up of dissolution products in the sediment, which could otherwise slow down the silicate dissolution rate and cause precipitation of secondary minerals (Meysman and Montserrat, 2017). The advection of oxygen-rich water into the sediment

155   promotes oxic mineralization of organic matter and reoxidation of reduced compounds, which decreases the pore water pH (Rao et al., 2014; Silburn et al., 2017; Wallmann et al., 2008; Widdicombe et al., 2011), which enhances the silicate dissolution (Rimstidt et al., 2012). In the *cohesive sediment scenario* (Fig. 2d), fine silicate particles are mixed into cohesive, fine-grained sediments where biotic processes can enhance the dissolution. Bioirrigation can flush out dissolution products and introduce oxygen into the sediment which in these generally organic-matter rich sediments, leads to a large pH decrease compared to the

160   overlying water (Aller, 2014; Silburn et al., 2017; Widdicombe et al., 2011). Macrofauna could also speed up the dissolution of silicate minerals through ingestion due to high enzymatic activity and low pH in the guts, combined with mechanical

abrasion (Meysman and Montserrat, 2017). In cohesive sediments, the pore water pH can also be lowered by the activity of certain microbes (e.g. cable bacteria, Meysman, 2018; Pfeffer et al., 2012). As detailed below, very little *in situ* data on the strength and efficiency of the different processes contributing to this benthic weathering engine are yet available. As a result, it is unclear which of the three scenarios (and hence which type of sediment locations) is the most promising for mERW.
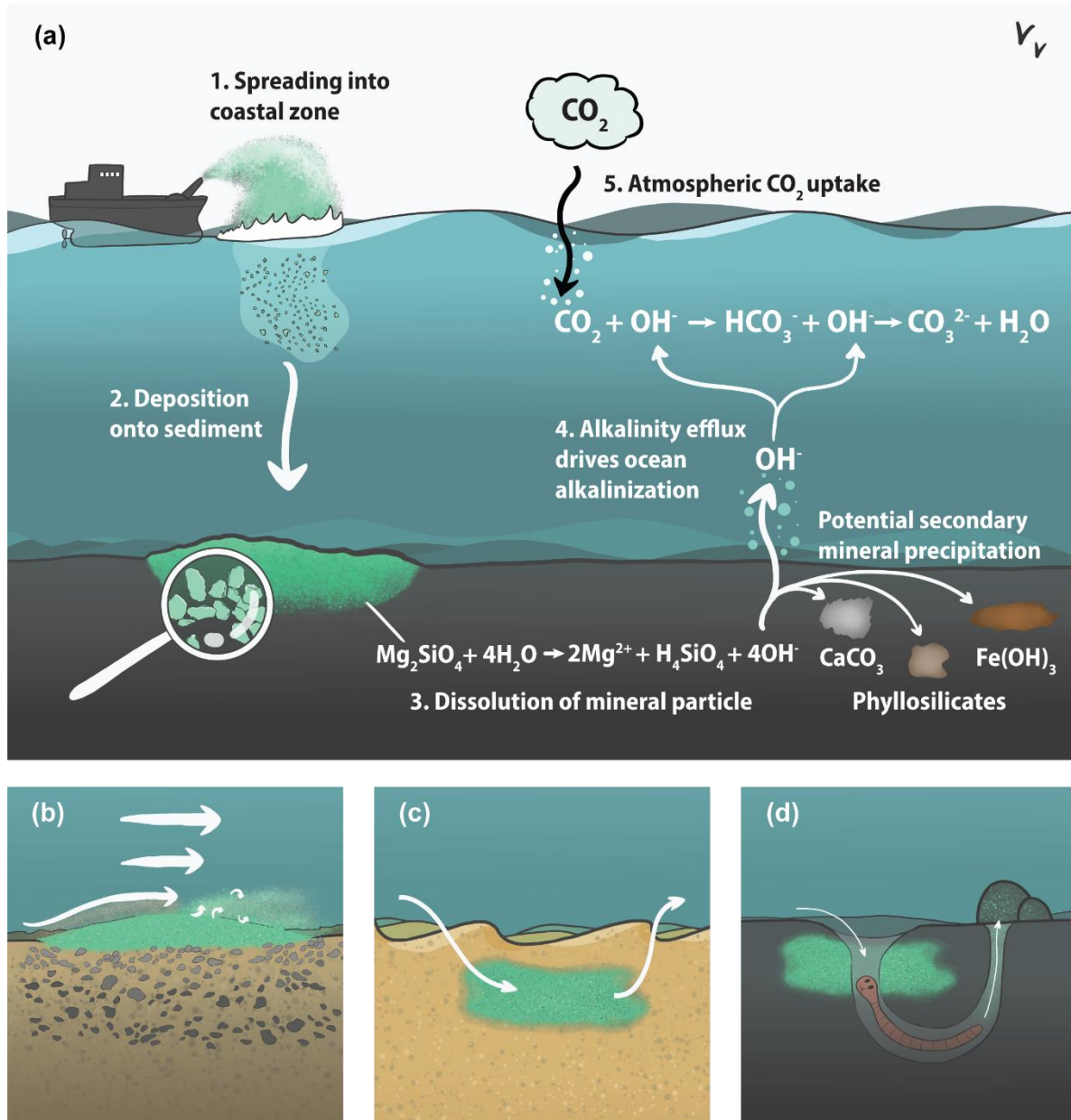
Figure 2. Principle of marine enhanced rock weathering (mERW) as a method for ocean alkalinity enhancement, including suggested application scenarios (Meysman and Montserrat, 2017). (a) Schematic overview of mERW: (1) Finely ground particles of a fast-

weathering silicate mineral (e.g. olivine) are spread in the coastal zone. (2) The silicate minerals are deposited onto or mixed into the sediment. (3) The silicate minerals dissolve, releasing alkalinity (here depicted as OH^-) to the pore water. (4) Alkalinity is either transported from the sediment to the overlying water, leading to ocean alkalinity enhancement, or is trapped in the sediment by secondary reactions. (5) Upon alkalinity addition, the seawater carbonate system re-equilibrates with the atmosphere, leading to an uptake of CO_2. (b) Bedload application scenario. Silicate minerals are deposited on top of the sediment, allowing bedload transport to naturally grind the grains to smaller sizes. (c) Permeable sediment application. High advective flows flushing the pore water and preventing the buildup of weathering products. (d) Cohesive sediment application. Bioirrigation leads to flushing of the pore water, and oxic mineralization processes lower the pH, which increases the silicate mineral dissolution rate. The thickness of the white arrows represents the force of water movement.

1.4 Scope of this review

This review focuses on mERW using olivine, which is the mineral that to date has been given the most attention in this context. In recent years, the mERW literature has discussed various aspects of enhanced olivine weathering, such as rock grinding requirements (Hangx and Spiers, 2009; Strefler et al., 2018), application areas and CO_2 sequestration efficiency (Bertagni and Porporato, 2022; Köhler et al., 2010; Moosdorf et al., 2014), life cycle analysis (Foteinis et al., 2023), secondary precipitation and dissolution reactions (Flipkens et al., 2023b; Fuhr et al., 2022; Montserrat et al., 2017; Rigopoulos et al., 2018), olivine dissolution rates (Hangx and Spiers, 2009; Heřmanská et al., 2022; Oelkers et al., 2018; Rimstidt et al., 2012), and ecotoxicological and ecological impacts (Bach et al., 2019; Flipkens et al., 2021, 2023a; Li et al., 2024). No data is yet available from mesocosm experiments or large-scale *in situ* pilots. The first mERW mesocosm experiments and field trials are currently being planned or are in the first stage of execution (e.g., Cornwall, 2023; USGS, 2023; Vesta, 2023), but no peer-reviewed publications have yet emerged on their outcomes. Therefore, the information currently available on mERW is either deduced from laboratory-scale dissolution experiments or based on modeling, raising the question to what extent these results can be confidently extrapolated to a real-world application. Dissolution experiments are typically performed under high fluid-to-mineral ratios, which is the opposite of natural sediments. Several studies have investigated olivine dissolution in artificial seawater (Fuhr et al., 2022; Montserrat et al., 2017; Rigopoulos et al., 2018), while fewer studies have used natural seawater (Flipkens et al., 2023b; Montserrat et al., 2017), and only three studies include sediment (Bach, 2024; Fuhr et al., 2023, 2024). While small-scale experiments in benchtop reactors or microcosms are key to constraining specific parameters and attaining detailed process knowledge, they do not replicate the physical and biological transport and biogeochemical reactions within the natural seafloor. Therefore, a critical challenge for olivine-based mERW is the lack of information obtained from suitably large-scale experiments that are performed under *in situ* conditions, which is essential for assessing its real-world applicability (Cyronak et al., 2023; Meysman and Montserrat, 2017; Renforth and Henderson, 2017; Riebesell et al., 2023). Consequently, critical questions remain regarding the feasibility, efficiency, and ecosystem impacts of olivine-based mERW.

In this review, we summarize recent research advancements seen through the lens of practical implementation of olivine-based mERW. Compared to previous reviews on mERW (Vandeginste et al., 2024; Wang et al., 2023), we concentrate on the context of coastal sediments since the conditions within this application environment are central to the outcome of mERW. Our focus is on predictability: given a target site in the coastal ocean, how confidently can we predict the olivine dissolution rate and the associated rate of alkalinity release and CO_2 sequestration? What aspects and parameters need consideration, and which are

currently uncertain (Table 2)? What aspects need specific consideration when performing future mesocosm pilots and field
trials? Compared to previous work on mERW, we specifically consider the heterogeneity of sediments within the coastal ocean
and hence the impact of sediment texture. We direct our attention to the various parameters that determine mineral dissolution
rates in different types of coastal sediments and we evaluate the ensuing CO_2 sequestration during olivine-based mERW. Our
goal is to bridge the gap between the experimental laboratory studies that have been conducted so far and the real-world
environment. We review the importance of processes that could hamper the efficiency of mERW (e.g., cation-depleted surface
layers, secondary mineral formation, pore water saturation) and highlight aspects that demand further scrutiny in future
experiments and field trials. Finally, we discuss some issues relevant to efficient monitoring, reporting, and verification (MRV)
of mERW applications.

Table 2. Overview of parameters and terminology used in the manuscript.

Symbol	Parameter	Value
A_0	Pre-exponential factor Arrhenius equation (mol m^{-2} s^{-1})	
A_{BET}	BET measured specific surface area (m^2 g^{-1})	
A_{geo}	Geometric specific surface area (m^2 g^{-1})	
A_{surf}	Specific surface area (m^2 g^{-1})	2–8
a_{H_2O}	Water activity (unitless)	
$C_{mineral}$	Mineral content of sediment at a given time (g mineral m^{-2} seafloor)	
D_e	Equivalent grain diameter (m)	
D_{max}	Maximum grain size in grain size interval (m)	
D_{min}	Minimum grain size in grain size interval (m)	
E_a	Activation energy of olivine dissolution in Arrhenius equation (kJ mol^{-1})	70.4 (pH < 5.6), 60.9 (pH > 5.6) [1]
k_d	Intrinsic dissolution rate constant of olivine (mol m^{-2} s^{-1})	
$L_{mineral}$	Mineral loading, $C_{mineral}$ at t$_0$ (g mineral m^{-2} seafloor)	
M_{CO_2}	Molar mass of CO_2 (g mol^{-1})	44.01
M_{FAY}	Molar mass of fayalite (g mol^{-1})	203.77 [2,3]
M_{FOR}	Molar mass of forsterite (g mol^{-1})	140.69 [2,3]
$M_{olivine}$	Molar mass of olivine (g mol^{-1})	140.69–203.77 [2,3]
P_{CO_2}	CO_2 capture potential (g CO_2 sequestered g^{-1} dissolved olivine)	
R	Universal gas constant (kJ K^{-1} mol^{-1})	8.314 x 10^{-3}
$F_{mineral}$	Areal mineral weathering rate (g mineral dissolved m^{-2} seafloor yr^{-1})	
F_{A_T}	Areal alkalinity release rate (mol alkalinity m^{-2} seafloor yr^{-1})	
F_{CO2}	Areal CO_2 sequestration rate (g CO_2 m^{-2} seafloor yr^{-1})	

R_{diss}	Specific mineral dissolution rate (g mineral dissolved g^{-1} mineral present yr^{-1})	
R_S	Grain roughness (unitless)	2–8
T	Temperature (K, C°)	
$V_{olivine}$	Molar volume of olivine (m^3 mol^{-1})	4.365×10^{-5}[2]
x_{FAY}	Mole fraction fayalite in olivine (unitless)	0.07–0.20
x_{inert}	Mass fraction inert minerals in dunite source rock (unitless)	0–0.1
η_{A_T}	Alkalinity transfer efficiency (unitless)	0–1
γ_{A_T}	Alkalinity production factor (unitless)	0–1
ρ_{CO_2}	CO$_2$ sequestration efficiency (mol CO$_2$ mol^{-1} alkalinity)	0.75–0.90[4,5]
φ	Fraction forsterite in particular grain diameter class	
Ω	Saturation index of mineral dissolution reaction (unitless)	0–1

[1](Rimstidt et al., 2012), [2](Deer et al., 2013), [3](Flipkens et al., 2021), [4](Bertagni and Porporato, 2022), [5](Schulz et al., 2023)

2 Olivine rocks and their availability

2.1 Olivine composition and source rocks

Olivine (Mg$_{(2-x)}$Fe$_x$SiO$_4$) constitutes a common group of igneous minerals, with compositions ranging from the magnesium
220 endmember forsterite (Mg$_2$SiO$_4$, M_{FOR} = 140.69 g mol^{-1}) to the iron endmember fayalite (Fe$_2$SiO$_4$, M_{FAY} = 203.77 g mol^{-1})
(Deer et al., 2013; Kremer et al., 2019). The molar mass of olivine ($M_{olivine}$) hence reflects the ratio between forsterite and
fayalite, with $M_{oli} = (1 - x_{FAY}) M_{FOR} + x_{FAY} M_{FAY}$, where x is the molar fraction of fayalite. Olivine also contains trace
metals, most notably, nickel (Ni) and chromium (Cr). Ni substitutes the divalent cations in olivine (Mg^{2+}, Fe^{2+}), and its content
ranges from 0.2–1.2 mol% (Keefner et al., 2011; Montserrat et al., 2017; Santos et al., 2015). Cr is typically present as chromite
225 (FeCr$_2$O$_4$) inclusions at lower concentrations of 0.02–0.66 mol% (Deer et al., 2013; Flipkens et al., 2021). The fate of these
metals upon dissolution and their potential impact on marine ecosystems remains an important topic of research for mERW
(Bach et al., 2019; Flipkens et al., 2021, 2023a; Foteinis et al., 2023), but falls outside of the scope of this review.
Olivine is one of the most rapidly weathering silicate minerals (Table 1) due to its structure, which consists of independent
silicate tetrahedra (SiO$_4$) linked by relatively weak Mg/Fe-O bonds (Sun and Huggins, 1947). This structure differs from most
230 other silicate minerals, in which SiO$_4$ tetrahedra are connected through a Si-O-Si bond, which has a three times greater bond
strength and hence is much harder to break (Velbel, 1999). Once the metal ion (Mg^{2+}/Fe^{2+}) in olivine is mobilized, the SiO$_4$
tetrahedra are also liberated and move into solution as dissolved orthosilicic acid, Si(OH)$_4$ (Oelkers et al., 2018).
Olivine is a major constituent of many ultramafic and mafic igneous rocks such as gabbro, peridotite, and basalt, where it
coexists with plagioclase and pyroxene (Deer et al., 2013; Klein et al., 2002). Because olivine is so easily altered by weathering,
235 it is not commonly found at the Earth's surface (Delvigne et al., 1979; Wilson, 2004). The highest concentration of olivine is
found in peridotite, which is an umbrella term for ultramafic rocks containing at least 40 weight% olivine (Fig. 3a). Peridotite

is further divided into dunite, harzburgite, wehrlite, and lherzolite, based on the relative abundance of olivine relative to orthopyroxene and clinopyroxene (Fig. 3a). Dunite contains over 90 weight% olivine by definition, and is, therefore, the most relevant peridotite rock for mERW (Caserini et al., 2022; Deer et al., 2013; Le Maitre et al., 2002). When using dunite as the olivine source rock, the mass fraction of inert minerals (x_{inert}) thus ranges between 0 and 0.10.

Dunite rocks with a high forsterite content are preferred for mERW. The ferrous iron (Fe^{2+}) produced when fayalite dissolves, will precipitate back as iron (Fe^{3+}) (hydr)oxides upon contact with O_2, which consumes any alkalinity produced during fayalite dissolution (Griffioen, (2017), section 3.2.2). Therefore, fayalite does not contribute to CO_2 drawdown. Typically, the forsterite fraction of olivine is substantially higher than the fayalite fraction, with x_{FOR} values of 0.80–0.88 in Fe-rich dunites and 0.88–0.94 in Mg-rich dunites, respectively (Ackerman et al., 2009; Deer et al., 2013; Harben and Smith, 2006; Rehfeldt et al., 2007; Su et al., 2016).

2.2 Availability of olivine

Olivine deposits are typically found at ultramafic intrusions (e.g. Norway, Germany), ophiolite complexes (e.g. Greece, Italy, Turkey), alpine peridotites emplaced along thrust faults (e.g. Italy, Spain), rift zones/ basalts of mid-ocean ridges (e.g. Iceland), and volcanic xenoliths (e.g.German Eifel and Kaiserstuhl, Iceland) (Harben and Smith, 2006; Kremer et al., 2019) (Fig. 3b–3c). Large dunite reserves are found within the Fjordane Complex, Norway (>2 Gt), the Piedmont region in Italy (650 Mt), Horoman Hill in Japan (100 Mt), and the Xixia and Yubian Counties in China (9 Mt) (Caserini et al., 2022; Harben and Smith, 2006). In the United States, a large dunite deposit (200 Gt) is present at Twin Sister Mountain (Caserini et al., 2022; Goff et al., 2000; Kremer et al., 2019), and a smaller one (300 Mt) in North Carolina (Caserini et al., 2022; Goff and Lackner, 1998). Dunite deposits are commercially exploited at several locations across the globe, as olivine is used as a slag conditioner in steel production to improve the performance and lifespan of the steel melting furnace (Harben and Smith, 2006). Established mining reserves for dunite amount to a few tens of gigatonnes (Gt), while potential resources are estimated at a few hundreds of Gt (see supplementary file 2, Harben and Smith 2006, and Caserini et al. 2022). For reference, the global reserves for wollastonite have been estimated at ~500 Mt, with purities of 40–96 weight% (Robinson et al., 2006), and are hence considerably smaller than those of olivine. At a theoretical CO_2 capture potential of 1.25 g CO_2 per g of forsterite dissolved (Hartmann et al., 2013), the currently exploited dunite reserves translate to a total CDR capacity of >50 Gt CO_2, which can increase up to a few hundred Gt if new mining deposits are exploited. The CDR potential for olivine could thus be considerable but note that the total CDR requirement over the 21st century to reach the Paris agreement targets is estimated at 400–1000 Gt CO_2 (Minx et al., 2018; Riahi et al., 2021; Rockström et al., 2017), which underlines to the extraordinary scale of the climate challenge. Therefore, olivine-based mERW should be considered within a portfolio of parallel CDR approaches. The global production rate of olivine sand is currently ~8 Mt per year (Harben and Smith, 2006), so this production rate would have to increase substantially to enable large-scale mERW. Ideally, olivine for mERW should be sourced close to the deployment location, as large transport distances considerably impact the environmental sustainability of mERW (Foteinis et al., 2023). The type of transport also matters, with overland transport via road and rail being 9 and 3 times more CO_2 intensive than

270 maritime transport (Renforth, 2012). Potential prime candidate sources for olivine rock are therefore large mines close to the sea (e.g. Åheim mine – Norway).
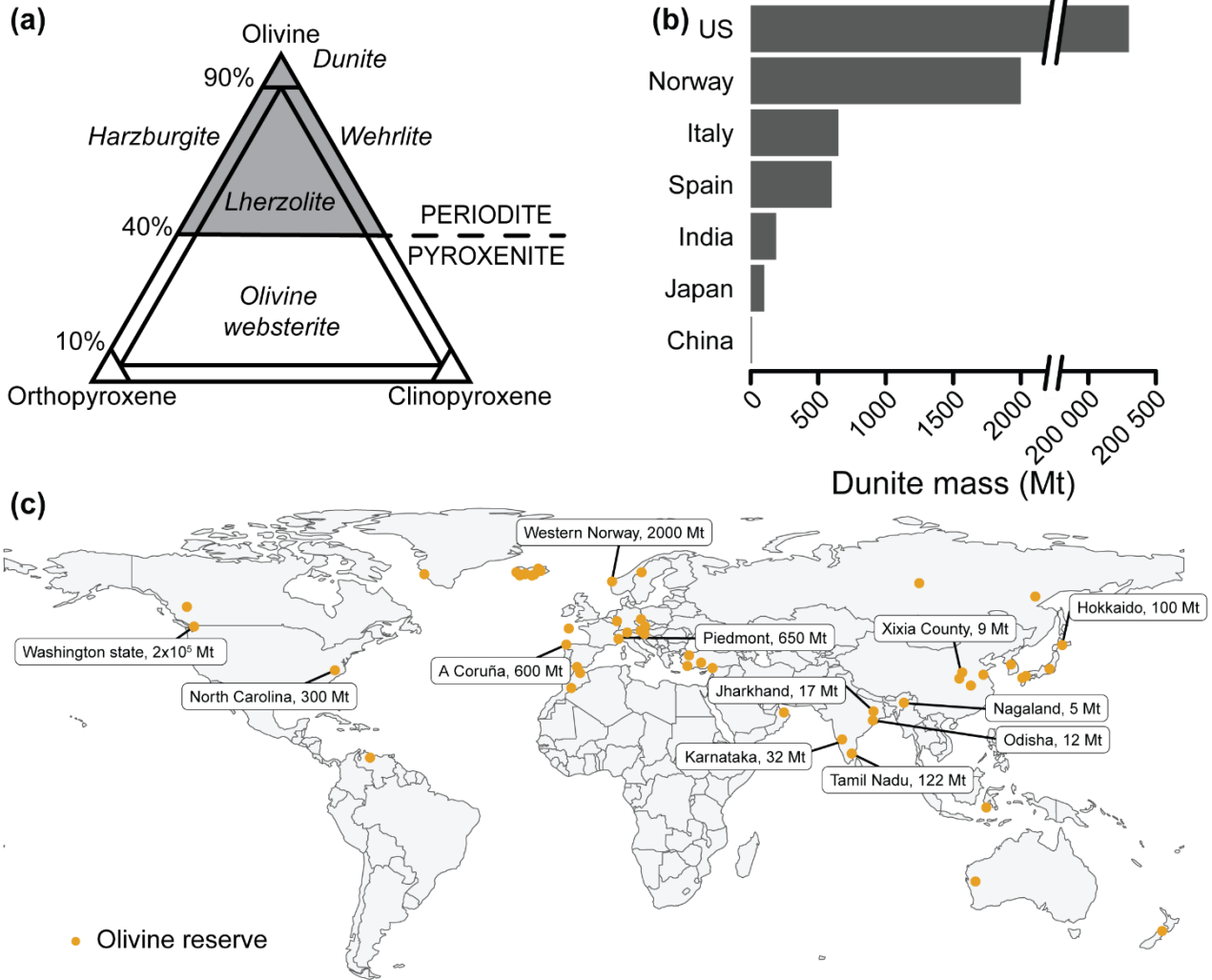
Figure 3. Olivine classification and occurrence around the globe. (a) Ternary plot for rock composed of olivine, orthopyroxene, and clinopyroxene. The peridotite group (grey) contains at least 40 weight% olivine. Dunite contains at least 90 weight% olivine. (b) The
275 **seven countries with the largest known dunite reserves. The best available reservoir estimate is given; the precise amount is uncertain. (c) Global map of locations with known dunite deposits (non-exhaustive). When known, the size of the deposit is displayed. A list of references and details is found in supplementary file 2.**

3 Factors affecting the CO_2 sequestration rate during mERW

The entire process of mERW can be quantitatively described as a six-step process (Fig. 2a): (1) production of olivine sand from olivine rich source rock (2) transport of the project site, (3) spreading and deposition onto the seabed (4) mineral dissolution, (5) alkalinity release to the overlying water, and (6) CO_2 sequestration at the air-sea interface. In the dissolution step, the olivine sand deposited during mERW will react on top of or within the seabed. The areal weathering rate (g mineral dissolved m^{-2} seafloor per unit of time) is provided by the rate expression (Meysman and Montserrat, 2017):

$$F_{\text{mineral}}(t) = -R_{\text{diss}}(t)C_{\text{mineral}}(t) \tag{1}$$

The specific mineral dissolution rate R_{diss} denotes the amount of source mineral that is lost per unit of time (g mineral dissolved g^{-1} mineral present yr^{-1}), while the mineral content C_{mineral} represents the amount of olivine sand that is present per unit of application area at a given time t (g mineral m^{-2} seafloor). The mineral loading $L_{\text{mineral}} = C_{\text{mineral}}(t_0)$ represents the amount of olivine sand initially deposited. When feedstock is utilized that contains an assemblage of different alkalinity-producing minerals (e.g. basalt), each mineral will be defined by its specific dissolution rate R_{diss}. The overall R_{diss} for the feedstock can be calculated by weighted averaging of the mineral-specific R_{diss} values using the mass ratios.

The weathering process will generate a certain amount of alkalinity (A_T) that escapes across the sediment-water interface towards the overlying seawater. The areal alkalinity release rate (mol alkalinity m^{-2} seafloor per unit of time) is linked to the areal weathering rate by:

$$F_{A_T} = 4\gamma_{A_T} \left(-\frac{1}{M_{\text{olivine}}} \cdot (1 - x_{\text{inert}}) \cdot F_{\text{mineral}} \right) \tag{2}$$

The alkalinity production factor γ_{A_T} (unitless) denotes how much alkalinity is produced upon mineral dissolution, relative to complete dissolution of olivine (producing 4 mol alkalinity per mol olivine). This factor depends on the mechanism of dissolution (different end products of olivine weathering are possible) and any loss of alkalinity due to precipitation of secondary minerals (section 3.2). The factor x_{inert} represents the mass fraction of inert minerals in the source rock, i.e., accessory minerals that do not dissolve and generate alkalinity, while M_{olivine} denotes the molar mass of olivine. The areal alkalinity release rate F_{A_T} thus represents the alkalinity that effectively reaches the overlying water.

In the final step, CO_2 sequestration will occur at the air-sea interface. The areal CO_2 sequestration rate (g CO_2 m^{-2} seafloor per unit of time) can be described as:

$$F_{CO_2} = M_{CO_2} \cdot \rho_{CO_2} \cdot \eta_{A_T} \cdot F_{A_T} \tag{3}$$

Here, M_{CO_2} represents the molar mass of CO_2 (44.01 g mol^{-1}), ρ_{CO_2} denotes thermodynamic CO_2 sequestration efficiency, i.e., the amount of CO_2 sequestered upon adding one mole of alkalinity to seawater (mol CO_2 mol^{-1} alkalinity), and η_{A_T} represents the alkalinity transfer efficiency, the fraction of alkalinity that effectively equilibrates with the atmosphere (coastal waters can be downwelled to the deep ocean before full CO_2 equilibration with the atmosphere has taken place). By combining Eq. 1–3, the CO_2 uptake rate can be expressed as:

$$F_{CO_2} = P_{CO_2}(t)R_{diss}(t)C_{mineral}(t)$$

310 The CO_2 capture potential P_{CO_2} (g CO_2 sequestered g^{-1} dissolved mineral) specifies the mass of CO_2 sequestered from the atmosphere per unit mass of source rock dissolved and is formally defined as (Meysman and Montserrat, 2017):

$$P_{CO_2} = \frac{M_{CO_2}}{M_{olivine}} \cdot \rho_{CO_2} \cdot \eta_{A_T} \cdot 4\gamma_{A_T} \cdot (1 - x_{inert}) \tag{4}$$

In the following sections, we will systematically review all the parameters that control the CO_2 capture potential P_{CO_2} and mineral dissolution rate R_{diss}. All parameters are expressed for olivine-based mERW (summarized in Table 2).

315 **3.1 Olivine dissolution rate**

The olivine dissolution rate $R_{diss}(t)$ can be parameterized as:

$$R_{diss}(t) = k_d \cdot A_{surf}(t) \cdot M_{olivine} \cdot (1 - \Omega(t)) \tag{5}$$

Here, k_d is the intrinsic dissolution rate constant (mol olivine dissolved m^{-2} of olivine surface area yr^{-1}), A_{surf} is the specific surface area at a given time (m^2 g^{-1}), $M_{olivine}$ is the molar mass of olivine (g^{-1} mol), and Ω is the saturation state. Saturation

320 occurs when dissolution products build up in the pore water, eventually reaching thermodynamic equilibrium ($\Omega = 1$ meaning full saturation) and thus impeding further dissolution (Köhler et al., 2010). Montserrat et al. (2017) and Flipkens et al. (2023b) reported that saturation effects slowed down dissolution rates in some of their long-term laboratory experiments. Yet, little is known about how the saturation state impacts olivine weathering in the pore water of marine sediments. The three mERW application scenarios considered (Fig. 2b–d) all assume some form of continuous exchange of the (pore) water surrounding

325 the olivine, thereby preventing saturation effects. However, saturation effects are expected to occur in cohesive sediments with little advection or biological irrigation. Potential saturation effects on olivine dissolution in marine sediments hence comprise an important aspect of investigation in future studies. In the following sections, we discuss the factors affecting k_d and A_{surf}, and their effects on the olivine dissolution rate.

3.1.1 The intrinsic dissolution rate of olivine

330 Many studies have investigated the k_d value of forsterite in aqueous solutions with a high fluid-to-mineral ratio, thus enabling experimental conditions to remain far from thermodynamic equilibrium (Bailey, 1976; Blum and Lasaga, 1988; Chen and Brantley, 2000; Eriksson, 1982; Giammar et al., 2005; Golubev et al., 2005; Grandstaff, 1986; Hänchen et al., 2006, 2007; Hausrath and Brantley, 2010; Luce et al., 1972; Oelkers, 2001a; Olsen et al., 2015; Olsen and Donald Rimstidt, 2008; Pokrovsky and Schott, 2000; Prigiobbe et al., 2009; Rosso and Rimstidt, 2000; Shirokova et al., 2012; Siegel and Pfannkuch,

335 1984; Van Herk et al., 1989; Wogelius and Walther, 1991). The resulting data have been synthesized in several reviews (Heřmanská et al., 2022; Oelkers et al., 2018; Rimstidt et al., 2012). This interest in olivine dissolution kinetics is due to its relatively simple reaction mechanism, its potential role in CO_2 sequestration (Heřmanská et al., 2022; Oelkers et al., 2018; Rimstidt et al., 2012), and more recently in reconstructing the past climate on Mars (Gaudin et al., 2018; Hausrath and Brantley,

2010; Niles et al., 2017; Olsen et al., 2015). These studies show that k_d primarily is affected by pH and temperature (Brantley
340 et al., 2008; Crundwell, 2014; Heřmanská et al., 2022; Olsen, 2007; Pokrovsky and Schott, 2000; Rimstidt et al., 2012; Wogelius and Walther, 1991). The following empirical equations for the dissolution rate constant, valid between $0 < pH < 14$ and $0°C < T < 150°C$, have been provided (Heřmanská et al., 2022; Rimstidt et al., 2012):

$$\log(k_d) = 5.17(0.16) - 0.44(0.01)pH - 3675(47.0)1/T \qquad (pH < 5.6) \qquad (6)$$

$$\log(k_d) = 2.34(0.40) - 0.22(0.02)pH - 3179(143)1/T \qquad (pH > 5.6) \qquad (7)$$

345 It is important to note that k_d values are normalized to the specific surface area of the olivine grain (section 3.1.5), which is represented in two ways: either the actual surface area as estimated via Brunauer, Edward, and Teller (BET) analysis (A_{BET}) or the geometrical surface area (A_{geo}), which assumes that the dissolving grain is a perfect sphere. The choice of surface normalization procedure critically influences the resulting k_d values, as A_{BET} can be considerably larger than A_{geo}. The Rimstidt relations Eq. (6) and Eq. (7) are normalized using A_{BET}, so the resulting k_d values should not be compared with those
350 normalized using A_{geo} without proper conversion.

Here, we discuss the impact of pH and temperature on k_d (Fig. 4a), as well as the effect of salinity, due to its relevance for coastal environments. Some studies have also suggested that the CO_2 concentration can affect the dissolution rate of olivine at a pH higher than 6 (Pokrovsky and Schott, 2000; Wogelius and Walther, 1991). However, more recent studies found no explicit CO_2 effect when correcting for the change in pH caused by elevated CO_2 concentrations (Golubev et al., 2005; Prigiobbe et
355 al., 2009). As such, CO_2 appears to affect olivine dissolution only indirectly through a change in pH. Rates of k_d in Fig. 4 were compiled from Rimstidt et al. (2012) and Heřmanská et al. (2022), supplemented with additional data (Flipkens et al., 2023b; Gerrits et al., 2020; Hausrath and Brantley, 2010; Lunstrum et al., 2023; Montserrat et al., 2017; supplementary file 2). The 95% confidence interval (CI) around the value of k_d is large, spanning an order of magnitude at pH < 5.6 and several orders of magnitude at pH > 5.6 (Fig. 4a). This large spread in the data has previously been discussed by Oelkers et al. (2018)
360 and Rimstidt et al. (2012), who attributed it to mineral purity (pure olivine dissolves faster e.g. Golubev et al., 2005), initial

incongruent dissolution of olivine, lack of common data format and inconsistent reporting, differences in sample grinding and preparation, and most importantly, to inaccuracies in reactive surface area measurements (section 3.1.5).
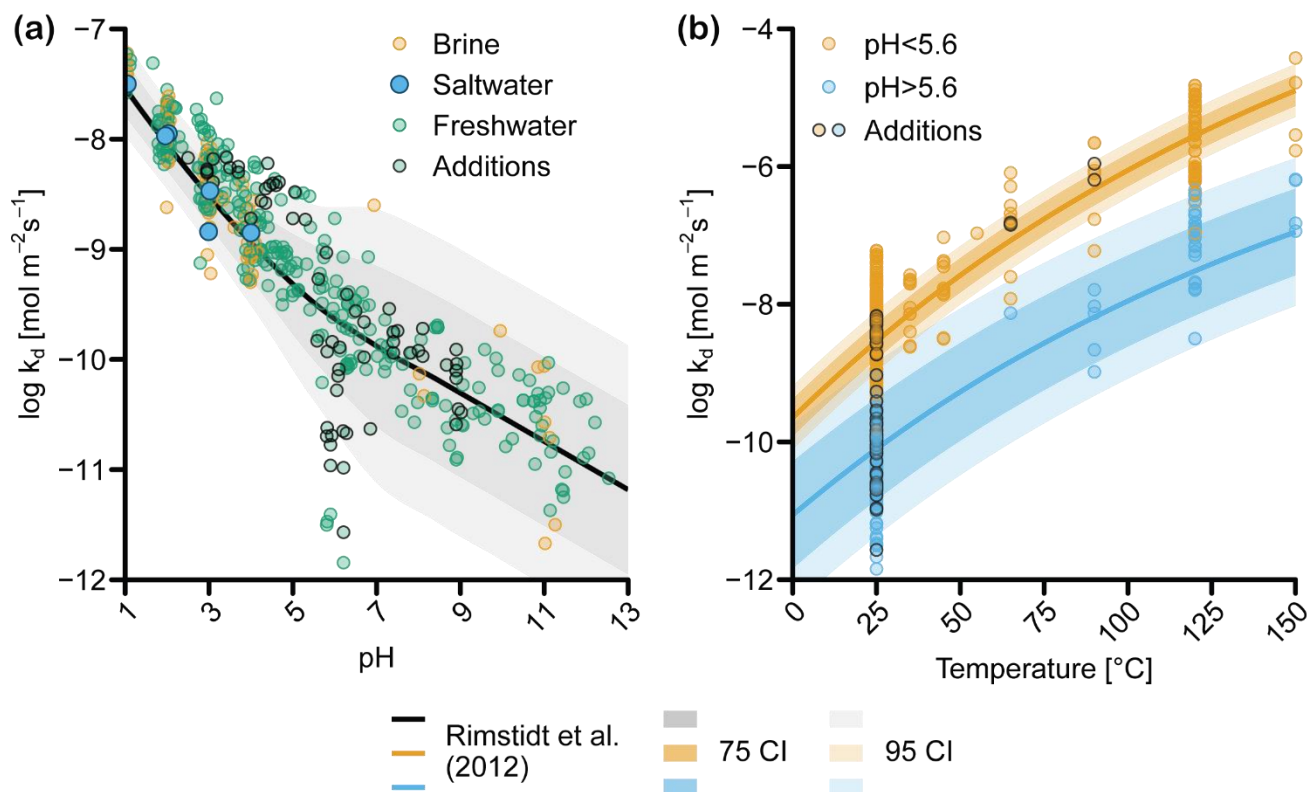
Figure 4. (a) Forsterite dissolution rates (k_d), adjusted to 25°C, as a function of pH according to the rate equations from Rimstidt et al. (2012). Data are normalized to BET surface areas and categorized according to salinity (freshwater < 0.6 mol l^{-1}, saline = 0.6– 0.85 mol l^{-1}, brine > 0.85 mol l^{-1}). Shadings show confidence intervals (CI) derived using the standard error for each parameter (supplementary file 1.2). (b) k_d as a function of temperature. The rate equation was solved for pH 3.13 and 8.22, respectively, which were the average pH values of experiments that Rimstidt et al. (2012) classified as "acidic" (pH < 5.6) and "basic" (pH > 5.6). "Additions" marks data from dissolution experiments where factors other than pH and temperature were investigated (e.g., the addition of dissolved organic matter, the addition of aluminum), which may have affected k_d (supplementary file 1.1).

3.1.2 Impact of pH on olivine dissolution

The olivine dissolution rate constant k_d follows a log-linear dependency on pH (Fig. 4a). Different mechanisms have been suggested to explain the observed change in dissolution rate between acidic and basic conditions. Pokrovsky and Schott (2000) argued that different reaction mechanisms occur at pH < 9 and pH > 9. For acidic and slightly alkaline conditions (pH < 9), Mg^{2+}/Fe^{2+} ions within the olivine are exchanged with two protons, creating a silica-rich, Mg/Fe-free protonated surface precursor complex followed by the sorption of one proton on two polymerized silica tetrahedra (Pokrovsky and Schott, 2000). A lower pH increases the concentration of free protons in solution, which can exchange with Mg/Fe in the olivine and accelerate

the release of silica tetrahedra and hence the dissolution of olivine (Oelkers et al., 2018; Pokrovsky and Schott, 2000). In basic conditions (pH > 9), silica would be preferentially released, and Mg/Fe sites hydrated, forming $(Mg/Fe)OH_2^+$ species that control the dissolution (Pokrovsky and Schott, 2000).

Rimstidt et al. (2012) also proposed two separate pH regimes, but with a transition at pH 5.6 rather than pH 9 (Fig. 4a). The dependency of k_d on pH is twice as strong at pH < 5.6 compared to pH > 5.6. While Rimstidt et al. (2012) point out that the apparent break in the data could be due to the relative paucity of rate measurements for pH > 6 and temperatures below 25°C, they also suggest that different mechanisms may drive the dissolution at low and high pH, leading to the two rate reactions presented in Eq. (6) and Eq. (7) (Rimstidt et al., 2012). Based on the dataset from Rimstidt et al. (2012), Crundwell (2014) proposed that an additional step occurs in basic and slightly acidic conditions (pH > 5.6), whereby H^+ ions absorb at the inner Helmholtz layer of the silicate mineral. This absorption would enable the release of Mg/Fe to the solution, after which the adsorbed H^+ ion can react with the silica tetrahedra to form H_4SiO_4, which goes into solution. This reaction mechanism explains the slope change at a pH~5.6 (Fig. 4a). In conclusion, there seems to be experimental and theoretical support for two dissolution mechanisms of olivine depending on pH regime, with considerably higher dissolution rates at lower pH (< 5.6).

The range of pH conditions relevant to mERW under field conditions is relatively narrow compared to the range shown in Fig. 4a. While the pH of coastal seawater is relatively high and shows minor variation (pH ≈ 7.9–8.3), the pH in coastal sediments is generally more acidic and also variable with depth (pH ≈ 6–8) (Cai et al., 1995; Pfeifer et al., 2002; Rao et al., 2012; Silburn et al., 2017; Widdicombe et al., 2011; Zhu et al., 2006). Olivine is therefore expected to show higher dissolution rates in the sediment compared to the water column (Meysman and Montserrat 2017). However, accurate descriptions of the spatial and temporal variability of the pore-water pH are currently lacking (Silburn et al., 2017). The pore-water pH is determined by microbial redox reactions, as well as mineral dissolution and precipitation, which in turn are controlled by sediment characteristics and the presence of burrowing fauna. Certain microbes, such as cable bacteria, can drastically change the pH profile (Meysman, 2018; Pfeffer et al., 2012) and have been found in previous mERW studies where they were suggested to lower the pH and increase the dissolution of $CaCO_3$ (Fuhr et al., 2023). Within the same sediment, spatial and temporal pH variations are the result of seasonal changes in the organic matter supply, which affects the sedimentary O_2 demand (Silburn et al., 2017; Widdicombe et al., 2011), alters the physical advection and biological irrigation (Meysman et al., 2007), and changes the microbial activity (Meysman et al., 2015). In addition to being a master variable for olivine dissolution, pH also determines the possibility of secondary reactions (e.g. sepiolite formation). The lack of data on olivine dissolution rates at pore-water pH and the absence of suitable spatial maps of sediment pH within coastal environments emerge as important research gaps that hamper the prediction of CO_2 sequestration by mERW. Careful monitoring of sediment pH during future field applications is required to designate the best application areas for mERW.

3.1.3 Impact of temperature on olivine dissolution

The k_d value increases with temperature, and this relationship is classically described via the Arrhenius equation (Casey and Sposito, 1992; Oelkers et al., 2018):

$$k_{\mathrm{d}} = A_0 \exp\left(\frac{-E_{\mathrm{a}}}{RT}\right) \tag{8}$$

where A_0 refers to the temperature-independent pre-exponential factor (mol m^{-2} s^{-1}), E_{a} stands for the apparent activation energy of olivine dissolution (J mol^{-1}), R is the gas constant (J K^{-1} mol^{-1}), and T is the temperature (K). The Arrhenius equation can be used to rescale k_{d} values to different temperatures via the relation (Montserrat et al., 2017):

$$415 \quad k_{\mathrm{d}2} = k_{\mathrm{d}1} \cdot \exp\left(\frac{E_{\mathrm{a}}}{R}\left(\frac{1}{T_2} - \frac{1}{T_1}\right)\right) \tag{9}$$

Past olivine dissolution studies have typically been conducted at temperatures of 25–125°C (Fig. 4b), from which E_{a} values of 70.4 kJ mol^{-1} for pH < 5.6 and 60.9 kJ mol^{-1} for pH > 5.6 have been derived (Rimstidt et al., 2012). However, there is a clear lack of rate studies within the environmentally relevant temperature range of 0–25°C, which reflects the natural variation of annual mean temperatures within the seafloor. The few experiments investigating dissolution below 25°C have found markedly

420   lower E$_{\mathrm{a}}$ values of 31–33 kJ mol^{-1} (Hausrath and Brantley, 2010; Niles et al., 2017), but these low-temperature activation energies were derived from experiments conducted in highly acidic conditions (pH < 2; Hausrath and Brantley 2010; Niles et al. 2017). Still, they suggest that the activation energy of 70.4 kJ mol^{-1} at pH < 5.6 used by (Rimstidt et al., 2012) may not hold for the temperature range 0–25°C. Only recently, have studies been conducted at environmentally relevant conditions (pH ~8 and temperature 0–25°C, e.g., Flipkens et al., 2023b; Fuhr et al., 2023, 2024). However, E$_{\mathrm{a}}$ was not reported in these studies,

425   and so the value of E$_{\mathrm{a}}$ is still uncertain under natural conditions, pinpointing an area for further research.

By applying the Arrhenius equation and using an apparent activation energy of 60.9 kJ mol^{-1} (Rimstidt et al., 2012), we find that olivine dissolves about 10 times faster at 25°C compared to at 0°C (Hangx and Spiers, 2009). From a mERW perspective, the geographical location is thus expected to impact the olivine dissolution rate profoundly. Spreading olivine in a polar region (temperature range 0–10°C) compared to application in tropical regions (temperature range 20–35°C) would decrease the

430   dissolution rate by a factor of 2.4–21.0. The sensitivity of k_{d} to temperature further implies that dissolution rates may vary with the seasons in temperate environments. This potentially temporal variability in the olivine dissolution rate complicates the MRV of mERW, as multiple measurements of olivine dissolution rates would be required at suitable temporal resolution throughout the seasonal cycle, thus increasing the costs of monitoring schemes.

3.1.4 Impact of salinity on olivine dissolution

435   The dissolution rate constant k_{d} decreases at high salinities (brine, ionic strength > 6 mol kg^{-1} solution), as the activity coefficient of water ($a_{\mathrm{H_2O}}$) is lowered when the ionic strength of an aqueous solution increases (Olsen et al., 2015; Prigiobbe et al., 2009). As $a_{\mathrm{H_2O}}$ expresses how easily the water can interact with the olivine, a high ionic strength of the solution indirectly affects the dissolution rate by lowering the "effective concentration" of the water needed to react with olivine. When correcting for the change in $a_{\mathrm{H_2O}}$, salinity does not noticeably affect the dissolution rate of olivine below an ionic strength of

440   12 mol kg^{-1} (for reference: open ocean seawater has an ionic strength of ~0.7 mol kg^{-1}; Olsen et al. 2015). It should be noted,

however, that most olivine dissolution experiments have been conducted in deionized water. Furthermore, olivine dissolution experiments at seawater salinities have mostly been conducted within the low pH range 1–4 (Fig. 4a). Accordingly, the effect of salinity on olivine dissolution at environmental field conditions (ionic strength 0–0.7 mol kg^{-1}, pH 6–8.3) has not been explicitly assessed, but salinity variations are unlikely to have a major effect.

3.1.5 Specific surface area

The specific surface area of the olivine grains is a crucial parameter since it is used to normalize k_d under the assumption that dissolution rates are surface-controlled (Brantley et al., 2008). Typically, surface areas are reported as either geometric (A_geo) or BET (A_BET) surface areas (Brantley et al., 2008; Brunauer et al., 1938; Rimstidt et al., 2012). When using A_geo, one assumes that the mineral grain adopts a spherical shape (Brantley et al., 2008). Accounting for spherical geometry, the geometric specific surface area is calculated for a grain size distribution consisting of n classes via (Flipkens et al., 2023b; Rimstidt et al., 2012):

$$A_\mathrm{geo} = \sum_{i=1}^{n} \left(\varphi_i \frac{6V_\mathrm{olivine}}{M_\mathrm{olivine} D_{\mathrm{e}_i}} \right) \tag{10}$$

Here, φ_i is the forsterite fraction of a certain grain diameter class i, V_olivine is the molar volume of forsterite (4.365×10^{-5} m^3 mol^{-1}), M_olivine is the molar mass of forsterite (140.69 g mol^{-1}), and D_e is the equivalent diameter (m) of a grain size interval (Tester et al., 1994):

$$D_\mathrm{e} = \frac{D_\mathrm{max} - D_\mathrm{min}}{\ln \left(D_\mathrm{max} / D_\mathrm{min} \right)} \tag{11}$$

In Eq. (11), the grain-size distribution is assumed to be constant over the given range. At small particle size intervals, the arithmetic mean of the maximum (D_max) and minimum (D_min) grain diameter of a particular grain size class will be close to D_e. For large intervals, D_e is smaller than the arithmetic mean since smaller particles contribute more to the area than large particles (Rimstidt et al., 2012; Tester et al., 1994).

The BET-based quantity A_BET is obtained by measuring the adsorption of a monolayer of inert gas (Kr, N$_2$) on a sample of grains (Brantley et al., 2008; Brantley and Mellott, 2000). Since the size of a water molecule is similar to that of N$_2$ and Kr, the BET method is considered to be a good proxy for characterizing the interaction between the mineral surface and water (Rimstidt et al., 2012). BET measurements are typically reported for the fresh olivine grains introduced at the start of the experiment, and because of the limited duration of experiments, it is assumed that the specific surface area does not markedly change (e.g. Hänchen et al. 2006; Pokrovsky and Schott 2000; Oelkers 2001b). However, under field conditions, the full dissolution of olivine sand may require 10-500 years, depending on the initial grain size. Accordingly, the evolution of A_BET as the grain dissolves is unknown, which must be considered in future long-term experiments.

The relation between A_geo and A_BET is given by the grain roughness (R_S), which is defined as (Brantley et al., 2008; Brantley and Mellott, 2000; Oelkers et al., 2018):

$$R_S = \frac{A_{BET}}{A_{geo}} \tag{12}$$

Fig. 5a shows the data distribution of R_S values as reported in the literature, which is largely based on Rimstidt et al. (2012) with a few additions. Following Rimstidt et al. (2012), we excluded data where R_S was larger than 10, as these values likely result from reading or calibration errors and retention of fine particles on the grain surfaces. Additionally, in our data

475 compilation, we omitted the data from Olsen et al. (2015), as they derived a BET value using an empirical rate equation from A_{geo} rather than a direct measurement. The R_S value in our compiled dataset ranges between 2 and 8, with a mean of 5.2 (Fig. 5a). Accordingly, there is considerable variation in grain roughness R_S between the olivine sand used in experiments. Moreover, there is no strong correlation between A_{BET} and A_{geo} (Fig. 5b). Overall, R_S tends to increase at smaller grain sizes (Strefler et al., 2018), albeit with substantial variability. Overall, the source of this variability remains poorly understood, but

480 it has been shown that the type of mill used to grind olivine source can significantly alter grain roughness R_S, providing highly different A_{BET} values for the same A_{geo} (Summers et al., 2005). The lack of a clear empirical relation between A_{BET} and A_{geo} complicates model-based predictions of the dissolution rate in future mERW applications. Therefore, an accurate characterization of R_S is highly advisable in future mERW experiments and applications. This issue also highlights the importance of a consistent normalization of reported dissolution rate constants k_d. Rimstidt et al. (2012) argued that

485 geometric-based normalization of dissolution rates can be useful for practical reasons, as it reduces analysis costs and avoids errors during BET measurements. However, using the actual A_{BET} value is advantageous due to the poor predictability of R_S.
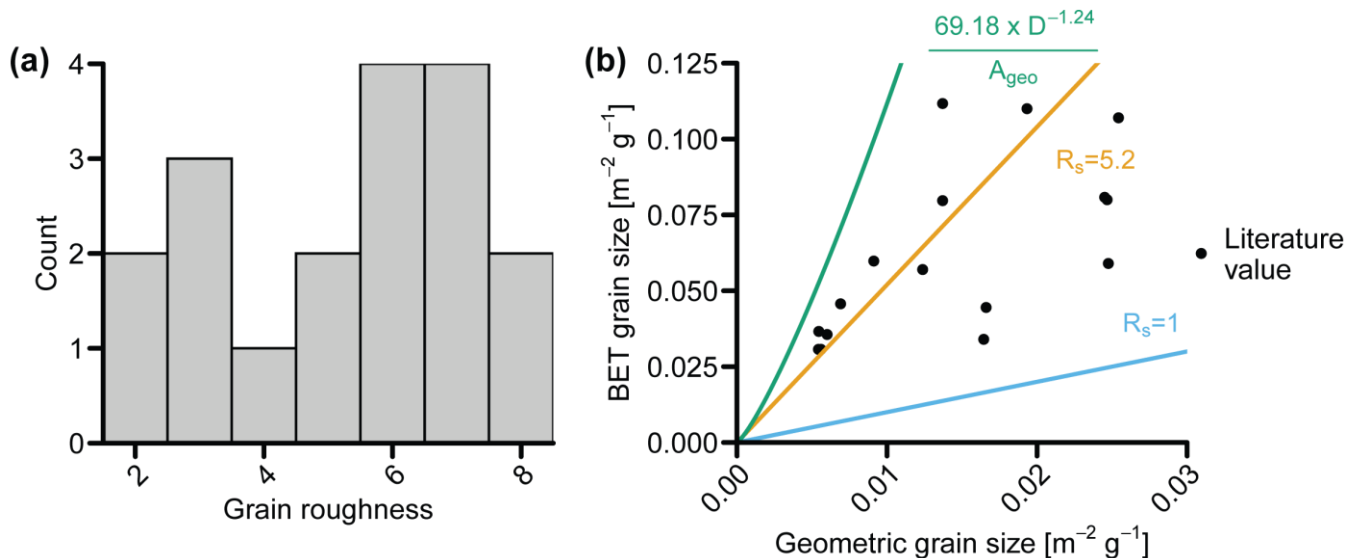
Figure 5. (a) Histogram of grain roughness (R_S) values in the compiled literature (supplementary file 2). (b) Relationship between
490 **the geometric surface area (A_{geo}) and BET surface area (A_{BET}). The empirical equation from Strefler et al. (2018) (in green) , where D is the grain diameter (µm), corresponds to an average $R_S \sim 12$. $R_S = 5.2$ is the mean grain roughness in the compiled literature, $R_S = 1$ shows the relationship for a perfect sphere.**

Furthermore, it should be noted that the link between specific surface area and mineral reactivity can change with time. In the olivine dissolution experiments conducted by Grandstaff (1978), A_{BET} increased substantially over five days (pH = 2.6) as etch pits and cracks formed. These dissolution features have also been found in naturally weathered olivine (Velbel, 2009) as well as laboratory olivine dissolution experiments (e.g. Flipkens et al. 2023b), and hence, the assumption that A_{BET} remains constant in time throughout long-term mERW applications is likely not valid. Interestingly, this large increase in BET was not accompanied by a concurrent increase in dissolution rate (Grandstaff, 1978), highlighting that there can be an increase in the total surface area while the reactive surface area stays the same. Rimstidt et al., (2012) identified this inconsistency as the major reason for the large data spread found between dissolution experiments (Fig. 4a). Unfortunately, temporal variation in reactive surface area is not easily monitored (Brantley et al., 2008; Oelkers et al., 2018; Rimstidt et al., 2012). Potentially, insight into the evolution of the reactive surface area over the whole weathering trajectory might be attained by looking at natural deposits of olivine sand with different ages (e.g. the older olivine deposit at Papakōlea beach in Hawaii versus the much younger Tremblet Beach in La Reunion). Comparing A_{BET} and k_d values of freshly mined olivine with those of naturally occurring olivine sand could indicate how olivine weathering rates in mERW applications may be affected over longer time scales.

3.1.6 Passivating layers

Passivating layers are any coatings on the olivine surface, biogenic or inorganic, that slow down dissolution. Microbial biofilms growing on olivine grains have been found to weakly inhibit dissolution (Shirokova et al., 2012), and precipitation of secondary minerals (sections 3.2) may also create passivating layers (Béarat et al. 2006; Sissmann et al. 2013). The occurrence of amorphic passivating layers on olivine grains and their effect on dissolution has been discussed in detail elsewhere (Pokrovsky and Schott, 2000; Béarat et al., 2006; Daval et al., 2011; Sissmann et al., 2013; Johnson et al., 2014), and was also extensively covered in the recent review by Oelkers et al. (2018). Amorphic layers may form as Mg^{2+} is leached from the olivine surface, causing the remaining silica-rich layer to repolymerize and form an amorphous SiO_2 coating (Béarat et al., 2006; Oelkers et al., 2018). However, SiO_2 coatings are only inhibiting when Fe^{3+} (derived from the fayalite component of the olivine itself) is incorporated into their structure (Oelkers et al., 2018). Recent experiments indicate that microbial and fungal uptake of either Fe (Gerrits et al., 2020, 2021; Lunstrum et al., 2023; Torres et al., 2019), or Fe and Si (Li et al., 2024), can prevent the formation of these passivating layers and increase olivine weathering rates. However, when no Fe uptake occurs, the effect of microbial biofilms on dissolution is less conclusive but appears to be slightly inhibiting (Shirokova et al., 2012). Future studies should consider *in situ* microbial effects on olivine dissolution, which is likely relevant for weathering in natural systems.

In their olivine dissolution experiments in seawater, Montserrat et al. (2017) observed a decreased Mg-to-Si atomic ratio on the surface of reacted forsterite compared to the initial substrate, indicating that a Mg-leached layer had formed as was proposed by Hellmann et al. (2012) and Maher et al. (2016). In contrast, Fuhr et al. (2022) found no such Mg-depletion, postulating that the high Mg concentrations in their artificial seawater prevented depletion at the olivine surface. Flipkens et al. (2023) mimicked the wave action in the coastal zone by continuously rotating olivine sand to induce grain collision,

hypothesizing that grain abrasion could decrease the formation of passivating layers. These experiments revealed that physical agitation increases the olivine dissolution rate by a factor of 8–19 compared to stagnant conditions. However, Flipkens et al. (2023) only found slight variations in the Mg-to-Si atomic ratio on the olivine grain surface between treatments (with large variations on the same grain), indicating that the formation of Mg-depleted layers was minimal in both the stagnant and high rotation treatments. Flipkens et al. (2023) hence attributed most of the dissolution rate enhancement to water flushing rather than physical abrasion of the grain surface.

Until now, there is little knowledge on passive layer formation on olivine grains under *in situ* marine conditions relevant to mERW. Previous experiments reporting on passivating layer formation have been typically conducted in freshwater at elevated CO_2 pressure (135–250 bar) and temperature (60–185°C) (Béarat et al., 2006; Daval et al., 2011; Johnson et al., 2014; Maher et al., 2016; Sissmann et al., 2013). Consequently, the possibility of passive layer formation in coastal sediment conditions warrants further research. Several processes may potentially counteract such layer formation during mERW application. In the bedload scenario, olivine particles will be subjected to the action of waves and currents, possibly removing passivating layers (Flipkens et al., 2023b). Moreover, when olivine is applied in cohesive sediment, the particles may be ingested by infauna, which could prevent passivating layer formation (Meysman and Montserrat, 2017). Although initial studies suggest that substantial formation of passivating layers seems unlikely (Bach, 2024; Flipkens et al., 2023b; Montserrat et al., 2017), the formation of a thin cation-depleted layer cannot be completely ruled out. Future work should investigate the precise conditions under which these layers form and how they impact weathering rates (Montserrat et al., 2017; Oelkers et al., 2018; Palandri and Kharaka, 2004; Pokrovsky and Schott, 2000), as well as further quantify the effect of grain abrasion on passivating layer formation (Flipkens et al., 2023b). Likewise, the prevalence and effect of biofilm formation on olivine dissolution rates need to be addressed in future mERW studies.

3.2 Secondary mineral formation

Chemical weathering of olivine is commonly described as a reaction where pure forsterite completely dissociates into its constituent ions Mg^{2+} and SiO_4^{4-}, thus generating 4 moles of alkalinity per mole of olivine dissolved (Table 3) (Meysman and Montserrat, 2017; Oelkers et al., 2018; Schuiling and Krijgsman, 2006). However, the alkalinity production can be decreased by the formation of secondary minerals via (i) incomplete olivine dissolution and (ii) precipitation of dissolved weathering products (Bach, 2024; Flipkens et al., 2023b; Fuhr et al., 2022; Griffioen, 2017; Meysman and Montserrat, 2017; Montserrat et al., 2017; Rigopoulos et al., 2018) (Table 3). During incomplete dissolution, alteration products such as serpentine or assemblages of clay minerals (e.g. iddingsite and smectites) are formed directly from the olivine, resulting in a lowered (or null) alkalinity production. Olivine that has dissolved completely can in turn contribute to the build-up of dissolution products in the sediment and promote the precipitation of minerals (e.g., carbonates, iron minerals, clays), which consumes alkalinity generated from olivine weathering. The relative reduction of alkalinity generation through secondary mineral formation can be described by the alkalinity production factor γ_{A_T}, which ranges from 0–1 (Table 3). Both the formation of olivine alteration

products and the precipitation of minerals from dissolution products are regulated by kinetics, the availability of nucleation

560 sites, and the saturation state of a particular mineral, with the latter being strongly affected by the water exchange rate. These

reactions are not exclusive and can occur in tandem, meaning that the overall value of γ_{A_T} should represent the weighted

contribution of the relevant reactions to the alkalinity loss. Recently, several experiments have been conducted on olivine

dissolution in both artificial seawater (e.g. Montserrat et al. 2017; Rigopoulos et al. 2018; Fuhr et al. 2022) and natural seawater

(Flipkens et al., 2023b; Fuhr et al., 2024; Montserrat et al., 2017). These studies provide a first insight into the secondary

565 minerals that can form during enhanced olivine weathering. However, it is unclear to what extent the reaction conditions (e.g.

pH and chemical environment) utilized in these laboratory experiments are relevant for olivine dissolution in sediments, and

studies conducted on olivine weathering in sediment have so far not addressed this issue (Bach, 2024; Fuhr et al., 2023, 2024).

In the sections below, we discuss the likelihood of formation of different secondary minerals during mERW with olivine.

570 **Table 3. Reactions that can affect the alkalinity generation during mERW with olivine, where γ_{AT} is the fraction of alkalinity generated relative to complete olivine dissolution (value 0–1). [a]No alkalinity is produced, but the reaction leads to the formation of magnesium carbonate, directly sequestering 0.5 mol DIC per mol forsterite. [b]The reaction is unbalanced since iddingsite does not consist of a single phase and its composition varies. [c]The Fe^{2+} stems from fayalite, as olivine typically comprises of 6–20 mol% Fe. [d]Fayalite weathering and sulfate reduction each produce 2 moles of alkalinity per mole of iron (Fe^{2+}) and SO_4^{2-}, respectively. When**

575 **both Fe^{2+} and sulfide (H_2S) precipitate to form iron sulfide (FeS), 2 moles alkalinity are consumed. Thus, the net result is that 2 moles of alkalinity produced by fayalite weathering are maintained. [e]When calcium carbonate (CaCO3) is formed, 1 mol DIC is sequestered directly within the mineral. Therefore, if all alkalinity from olivine dissolution is consumed in carbonate precipitation, half of the CO₂ is sequestered compared to a situation without carbonate precipitation.**

Reaction	Mechanism	γ_{A_T}
Complete olivine dissolution[1]	$Mg_2SiO_4 + 4H_2O \rightarrow 4OH^- + 2Mg^{2+} + H_4SiO_4$	1
Serpentinization[2]	$Mg_2SiO_4 + \frac{4}{3}H_2O + \frac{1}{3}SiO_2 \rightarrow 0OH^- + \frac{2}{3}Mg_3Si_2O_5(OH)_4$	0
	$MgSiO_4 + \frac{3}{2}H_2O \rightarrow \frac{1}{2}Mg_3Si_2O_5(OH)_4 + \frac{1}{2}Mg(OH)_2$	0
	$MgSiO_4 + H_2O + \frac{1}{2}CO_2 \rightarrow \frac{1}{2}Mg_3Si_2O_5(OH)_4 + \frac{1}{2}MgCO_3$	0[a]
Iddingsitization[b,3,4]	$(Mg,Fe)_2SiO_4 \rightarrow 0OH^- + MgO \bullet Fe_2O_3 \bullet 3SiO_2 \bullet 4H_2O$	0
Saponite formation[5]	$0.15Ca^{2+} + 0.1Na^+ + 2.5Mg^{2+} + 0.8Fe^{2+} + 3H_4SiO_4 + Al(OH)_3 + 7HCO_3^- \rightarrow$ $Ca_{0.15}Na_{0.1}Mg_{2.5}Fe_{0.8}^{2+}Si_3AlO_{10}(OH)_2 + 7CO_2 + 10H_2O$	0.60
Sepiolite formation[5]	$4Mg^{2+} + 6H_4SiO_4 + 8HCO_3^- \rightarrow Mg_4Si_6O_{15}(OH)_2 + 8CO_2 + 15H_2O$	0.33
Iron oxide precipitation[c]	$Fe^{2+} + \frac{1}{4}O_2 + 2OH^- + \frac{1}{2}H_2O \rightarrow Fe(OH)_3$	0

| Sulfate reduction + iron sulfide precipitation[c] | $2CH_2O + SO_4^{2-} \rightarrow 2CO_2 + H_2S + 2OH^-$

 $Fe^{2+} + H_2S + 2OH^- \rightarrow FeS + 2H_2O$ | 1[d] |
| Carbonate precipitation | $Ca^{2+} + 2HCO_3^- \rightarrow CaCO_3 + CO_2 + H_2O$ | 0[e] |

[1](Meysman and Montserrat, 2017), [2](Deer et al., 2013), [3](Edwards, 1938), [4](Wilson, 2004), [5](Isson and Planavsky, 2018)

580

3.2.1 Formation of clay minerals

Clay minerals can form either through direct alteration of the olivine or through authigenic precipitation of dissolution products, also known as reverse weathering (Deer et al., 2013; Delvigne et al., 1979; Isson and Planavsky, 2018). The saturation state of the system, which is primarily driven by the water exchange, is critical for clay mineral formation. When rock-to-fluid

585 ratios are low, Mg^{2+} and Fe^{2+} from olivine dissolution escape into solution (Delvigne et al., 1979; Wilson 2004). When rock-to-fluid ratios are high, dissolution products are concentrated, and clay formation is promoted (Delvigne et al., 1979; Gaudin et al., 2018).

Serpentinization is an olivine alteration process in which forsterite is transformed into the clay serpentine, sometimes in parallel with the formation of brucite ($Mg(OH)_2$) or magnesite ($MgCO_3$) (Table 3) (Deer et al., 2013; Griffioen, 2017). No alkalinity

590 is formed during serpentinization $\left(\gamma_{A_T} = 0 \right)$, but precipitation of magnesite leads to direct sequestration of CO_2 in the mineral. In marine environments, serpentine is typically formed over a wide temperature range (50–600°C) in high-temperature hydrothermal systems, subduction zones, and mid-ocean ridges (Alt et al., 2012, 2013; Schwarzenbach et al., 2012). Serpentinization has also been found to occur at lower temperatures (from 200°C down to ~10°C) in hydrothermal deposits with high sulfide content, such as the Lost City hydrothermal field (Mid-Atlantic ridge) (Alt et al., 2012; Mével, 2003; Neubeck

595 et al., 2011).

Saponite (a smectite mineral, formerly classified as bowlingite) and iddingsite are often identified as alteration products of olivine, although saponite can also be formed through precipitation (Deer et al., 2013; Dehouck et al., 2016; Delvigne et al., 1979; Gaudin et al., 2018; Isson and Planavsky, 2018) . The formation of saponite reduces the alkalinity production to 2.4 moles alkalinity mol^{-1} olivine $\left(\gamma_{A_T} = 0.6 \right)$ and the formation of iddingsite does not lead to any alkalinity production $\left(\gamma_{A_T} = 0 \right)$

600 (Isson and Planavsky, 2018). The relative abundance of saponite and iddingsite is dependent on the oxidation state of Fe, with saponite being formed under non-oxidative conditions and iddingsite under oxidative conditions (Deer et al., 2013; Smith et al., 1987). Sepiolite has also been suggested to precipitate from olivine dissolution products (Griffioen, 2017) and reduces the alkalinity production to 1.32 moles alkalinity mol^{-1} olivine $\left(\gamma_{A_T} = 0.33 \right)$ (Table 3). Sepiolite formation has been observed in low-temperature systems, such as near hydrothermal vents, in marine and lacustrine sediments, and in volcanic deposits

605 (Mulders and Oelkers, 2020; Wollast et al., 1968). Sepiolite formation requires a high pH > 8 (Baldermann et al., 2018; Wollast et al., 1968) and elevated concentrations of dissolved Si and Mg^{2+} (Baldermann et al., 2018; Tosca and Masterson, 2014). Since seawater contains high concentrations of Mg^{2+} (0.05 mol kg^{-1}; Johnson et al., 1992), dissolved Si is generally the limiting

element for sepiolite formation in marine environments (Baldermann et al., 2018). However, even at a steady supply of dissolved Si (e.g., through silicate weathering or dissolution of biogenic opal) and at a high pH, precipitation of sepiolite remains slow (~10^{-12} mol s^{-1}) at ambient coastal seawater temperatures (Baldermann et al., 2018). In marine conditions, sepiolite formation is further impeded by the presence of sodium ions (Na^+), which affects the speciation of dissolved silicate, and by the presence of sulfate ions (SO_4^{2-}), which lowers the availability of free Mg^{2+} through the formation of $MgSO_4$ complexes (Baldermann et al., 2018; Tosca and Masterson, 2014).

Up until now, serpentine has not been found to form in olivine dissolution experiments using oxic seawater (Flipkens et al., 2023b; Fuhr et al., 2022; Montserrat et al., 2017; Rigopoulos et al., 2018), although both Fuhr et al. (2022) and Flipkens et al. (2023) calculated that serpentine was oversaturated throughout most of their experiments. However, serpentinization is unlikely during mERW as it typically occurs at temperatures much higher than in coastal systems (0–35°C). Serpentinization with magnesite production is particularly unlikely as this mineral typically does not form under ambient marine conditions (section 3.2.3), and brucite formation is unfavorable at pH values below 8 (Griffioen, 2017; Wollast et al., 1968). Fuhr et al. (2022) and Flipkens et al. (2023) also advanced that talc ($Mg_3Si_4O_{10}(OH)_2$) formation is possible. However, talc formation from olivine proceeds via (or co-occurs with) serpentine, and these reactions require high pressure and temperature (200–650°C; Bucher and Grapes 2011; Deer et al. 2013). As such, the formation of talc is unlikely in coastal settings. Little experimental data exists on the formation of saponite and iddingsite during olivine dissolution. Even though the formation of saponite and iddingsite during olivine dissolution in soils has been historically well-documented for soils (Baker and Haggerty, 1967; Brown and Stephen, 1959; Edwards, 1938; Eggleton, 1984; Sherman and Uehara, 1956; Smith et al., 1987; Sun, 1957; Wilshire, 1958), the process has not been investigated in seawater conditions. Model calculations have also shown sepiolite oversaturation in studies on olivine dissolution in seawater (Flipkens et al., 2023b; Fuhr et al., 2022; Rigopoulos et al., 2018), yet documentation of sepiolite formation remains inconclusive. Sepiolite has only been directly observed once (Rigopoulos et al., 2018), while another study found a mix of silicate-bearing phases precipitated on weathered olivine grains, potentially including sepiolite (Fuhr et al., 2022). In contrast, Montserrat et al. (2017) and Flipkens et al. (2023) found no phyllosilicate precipitates. Oelkers et al. (2018) suggested that sepiolite formation in the experiments by Rigopoulos et al. (2018) could have been provoked by the buildup of Mg^{2+} in the supernatant solution. However, this is unlikely due to the high background concentration of Mg^{2+} in seawater. Instead, a rapid pH increase (from 8 to >8.6) caused by rock flour addition may have caused the observed precipitation, since a pH increase from 8 to 9 can increase the sepiolite growth rates by an order of magnitude (Baldermann et al., 2018). Overall, due to the generally low pH of pore water and low ambient temperatures in coastal environments, sepiolite formation is unlikely during mERW application, but more targeted studies are needed to confirm this. While clay formation should be targeted by future mERW studies, they are unlikely to find well-crystalized clays. Instead, authigenic clay minerals are likely to appear as "poorly crystalline gels", which act as precursor complexes (Tosca and Masterson, 2014), similar to the observations by Rigopoulos et al. (2018).

3.2.2 Iron mineral formation

Dissolution of fayalite releases Fe^{2+} to the pore water, which in oxic environments spontaneously precipitates as iron (hydr)oxides during aerobic oxidation (Table 3) (Griffioen, 2017). Iron oxidation consumes 2 moles of alkalinity per mole of Fe^{2+}, equaling the alkalinity produced during fayalite dissolution ($\gamma_{A_T} = 0$). Assuming complete dissolution of olivine followed by precipitation of the 6–20 mol% Fe in olivine (Ackerman et al., 2009; Deer et al., 2013; Harben and Smith, 2006; Rehfeldt et al., 2007; Su et al., 2016) as iron oxides, 3.2–3.76 moles of alkalinity are produced per mol of olivine. The formation of iron (hydr)oxides has been confirmed in olivine dissolution experiments in seawater (Fuhr et al., 2022; Rigopoulos et al., 2018). Precipitation of iron (hydr)oxides is also expected from a thermodynamic perspective, as these experiments were conducted under well-oxygenated conditions. During mERW applications, well-flushed and well-oxygenated sediments are targeted to avoid porewater saturation effects, so the alkalinity reduction due to Fe oxidation from fayalite needs consideration.

If olivine particles are buried in deeper, anoxic sediment layers, the Fe^{2+} released from fayalite dissolution can react with H_2S and form iron sulfides (FeS_x, Table 3). Like iron oxide formation, the precipitation of the FeS_x consumes the alkalinity formed through fayalite dissolution. However, the alkalinity formed via sulfate reduction is preserved when H_2S is prevented from reoxidizing through trapping in the sediment (Hu and Cai, 2011; Middelburg et al., 2020), causing a net alkalinity production of 4 mol per mol olivine and thus giving a γ_{A_T} of 1. However, the fate of any FeS_x minerals produced must be closely scrutinized, as it will determine the permanence of the alkalinity produced. If the FeS_x comes into contact with O_2 (e.g. through bioirrigation or physical advection), they will be reoxidized, and the alkalinity produced during their precipitation will be consumed again (Schippers and Jørgensen, 2002). The long-term fate of ferrous iron released during mERW trials is not well constrained, and will most likely be strongly dependent on the application scenario (cohesive versus permeable). It is hence an important point of attention in future mesocosm experiments and field trials.

3.2.3 Stimulated precipitation and inhibited dissolution of carbonates

The release of alkalinity from olivine weathering increases the saturation state of carbonates, which can lead to precipitation of these minerals in the sediment or the water column. Carbonate precipitation consumes 1 mol of dissolved inorganic carbon (DIC) and 2 moles of alkalinity (Table 3), hence leading to the outgassing of CO_2 to the atmosphere (Wolf-Gladrow et al., 2007). In theory, different carbonate minerals can form. Given the release of Mg^{2+} and Fe^{2+} during olivine dissolution, the formation of magnesite ($MgCO_3$) and siderite ($FeCO_3$) needs consideration. However, $MgCO_3$ is unlikely to form during mERW in coastal sediments, as it typically only precipitates at elevated CO_2 pressure or temperature (60–100°C) (Griffioen, 2017; Saldi et al., 2009). Likewise, the formation of $FeCO_3$ requires particular environmental conditions, including anoxic but hydrogen sulfide (H_2S) free conditions with high concentrations of Fe^{2+} and a narrow pH window between 6.0 and 7.2 (Lin et al., 2020). Therefore, the most likely carbonates to precipitate are calcium carbonates ($CaCO_3$). Coastal waters are oversaturated with respect to $CaCO_3$ (Morse et al., 2007), and so there is concern that the addition of alkalinity through OAE could induce precipitation of the mineral (Hartmann et al., 2023; Moras et al., 2022). The saturation state with respect to $CaCO_3$

is highly dependent on the type of sediment. In more permeable, sandy sediments, oxic respiration processes lower the pH and can result in undersaturation and dissolution of $CaCO_3$ (Milliman and Droxler, 1996; Morse and Mackenzie, 1990; Rao et al., 2014). While dissolution of $CaCO_3$ may be considerable in cohesive sediments (e.g., Rao et al., 2014), this process can be counteracted by anoxic respiration processes that produce alkalinity and elevate the saturation state of $CaCO_3$ (Berner, 1984; Turchyn et al., 2021). However, a high saturation state does not necessarily lead to $CaCO_3$ precipitation due to inhibitors such as phosphate and organic matter in the sediment (Morse et al., 2007; Turchyn et al., 2021). Flushing of the sediment through advection or bioirrigation also prevents alkalinity from building up (Rao et al., 2012).

Olivine dissolution experiments in seawater have generated mixed and conflicting results regarding the importance of secondary $CaCO_3$ formation. In some experiments, $CaCO_3$ formation was observed (Fuhr et al., 2022; Rigopoulos et al., 2018), while other experiments did not show any precipitation (Bach, 2024; Flipkens et al., 2023b; Montserrat et al., 2017). One factor causing $CaCO_3$ precipitation could be that the seawater was isolated from the atmosphere in some experiments (Fuhr et al., 2022; Rigopoulos et al., 2018), whereas no precipitation was observed in experiments where gas exchange was allowed (Flipkens et al., 2023b; Montserrat et al., 2017). The latter ensures that CO_2 can move into solution as alkalinity is produced, thus preventing a pH rise and resulting in $CaCO_3$ oversaturation. Another explanation for the varying results could be the use of different types of seawater in the experiments. The presence of phosphate may have inhibited $CaCO_3$ formation in experiments with natural seawater (Bach, 2024; Flipkens et al., 2023b; Montserrat et al., 2017), in contrast to experiments conducted with phosphate-free artificial seawater (Fuhr et al., 2022; Rigopoulos et al., 2018). As predicted by thermodynamic modeling (Griffioen, 2017), no magnesite ($MgCO_3$) has been detected in olivine dissolution experiments in seawater (Flipkens et al., 2023b; Fuhr et al., 2022; Montserrat et al., 2017; Rigopoulos et al., 2018). Siderite ($FeCO_3$) formation was not explicitly investigated in the experiments, but as noted above, this process is unlikely based on theoretical grounds.

Although mERW might not cause precipitation of $CaCO_3$ in the sediment, it could impede natural alkalinity production by inhibiting the dissolution of $CaCO_3$ already present in the sediment (Bach, 2024). As such, the alkalinity sourced from carbonate dissolution is substituted with alkalinity from olivine dissolution, so the alkalinity generated by mERW is no longer fully additional to the alkalinity efflux before mERW application. While the additionality problem may imply that mERW does not increase the sedimentary alkalinity release, the CO_2 sequestration potential still increases when alkalinity originates from olivine, as $CaCO_3$ dissolution results in a concomitant release of alkalinity and DIC, while no DIC is produced during olivine dissolution (Bach, 2024). The coastal sediments in which $CaCO_3$ dissolution is high are those where the pH is lowered due to oxic mineralization of organic matter, thus overlapping with the optimal environmental conditions for olivine dissolution. The additionality problem may thus be an issue for mERW in both the permeable and cohesive sediment application scenarios (Fig. 2c–d), in which the dissolution of olivine dissolution occurs at the location of carbonate dissolution. If areas with permeable or cohesive sediments are targeted for mERW, it should first be confirmed that they are not strong sources of alkalinity from natural $CaCO_3$ dissolution. However, the additionality problem should not be an immediate issue for the bedload application (Fig. 2b), as the olivine is weathering in seawater that is already oversaturated with respect to $CaCO_3$, and there is also an immediate dilution of the alkalinity.

In conclusion, the rate at which mERW applications influence natural alkalinity release from sediments imposes a major uncertainty on γ_{A_T}. The additionality problem could have profound implications for the location chosen for mERW application and the economics and MRV of a mERW project, as the net alkalinity generation must be quantified rather than the total sedimentary alkalinity release. Hence, future mERW experiments need to quantify the natural alkalinity production in control sediments and determine to what extent this process is affected by mineral addition.

mERW targets a slow release of alkalinity from the sediment to the water column, however, other OAE approaches, such as ocean liming and electrochemistry, target a fast, immediate release of alkalinity (Fig. 1). These fast-release approaches can result in substantial alkalinity increases at the local scale. In recent liming experiments, the addition of ~250 µmol kg^{-1} alkalinity on top of a seawater baseline of 2400 µmol kg^{-1} (a ~10% increase, equivalent to an aragonite saturation index of ~5) was delineated as a safe threshold to avoid CaCO$_3$ precipitation in the water (Moras et al., 2022). In contrast, the addition of 500 µmol kg^{-1} of alkalinity led to "runaway precipitation", a process where CaCO$_3$ precipitation continued until the aragonite saturation reached 1.8–2.0 and the alkalinity concentration had been reduced below the initial seawater values (Hartmann et al., 2023; Moras et al., 2022). However, the risk of runaway precipitation is small when using olivine for mERW. When applying olivine grains of 10 µm at a loading of 15 kg olivine m^{-2} in a very shallow system (1 meter of overlying water, equivalent to the 15 g l^{-1} used by, Montserrat et al., 2017), the alkalinity concentration in the overlying water increases by ~170 µmol kg^{-1} seawater over the course of a day (supplementary file 1.3). This alkalinity increase is well below what has been deemed safe in past run-away experiments (Moras et al., 2022). In reality, this alkalinity would not continue to build up in the overlying water but would be diluted, further minimizing the risk of immediate CaCO$_3$ precipitation in the overlying water. Finally, alkalinity generation through olivine addition could stimulate the growth of calcifying algae and lead to loss of alkalinity through increased biogenic CaCO$_3$ precipitation in the water column. However, while the addition of olivine appears to stimulate the growth of phytoplankton in general, there is a much more pronounced effect on silicifying algae (Li et al., 2024), which out-compete other phytoplankton such as calcifying coccolithophores (Bach et al., 2019; Li et al., 2024). These initial studies thus indicate that the risk of substantial alkalinity loss in the water column due to increased biogenic calcification is small.

3.2.4 Implications for mERW with olivine

Apart from the precipitation of Fe oxides following fayalite dissolution, experiments on olivine dissolution in seawater have so far provided little evidence of extensive secondary mineral formation via incomplete olivine dissolution or authigenic precipitation. In one instance, small amounts of sepiolite formation were reported (Rigopoulos et al., 2018), whereas no serpentinization has been observed (Montserrat et al., 2017; Rigopoulos et al., 2018; Fuhr et al., 2022; Flipkens et al., 2023b). Most mERW experiments have been conducted in oxygenated seawater and are not fully representative of sedimentary conditions (e.g. in terms of O$_2$ and pH), and studies in sediments under hypoxic-anoxic bottom water have not investigated the formation of secondary minerals (Fuhr et al., 2024). Most olivine dissolution experiments have also been conducted in closed systems, where reaction products are allowed to build up (e.g. Montserrat et al., 2017; Rigopoulos et al., 2018; Fuhr et al.,

2022). Under mERW application, the weathering will take place in an open environment. Reaction products from olivine weathering will be released into the pore water, which can then be flushed either through physical advection (wave or current action) or through bioirrigation (Meysman and Montserrat, 2017). It should be noted that Bach (2024) and Fuhr et al. (2023, 2024) included sediment in their ERW experiments; however, they did not specifically investigate secondary mineral formation. While the physiochemical conditions in coastal sediments seem unfavourable for the formation of serpentine, the formation of iddingsite and smectites (most notably saponite) could be relevant depending on flushing conditions, and their formation during mERW warrants further research. Similarly, the effect of olivine dissolution on the inhibition of natural carbonate dissolution may be important in cohesive and permeable sediments and should be investigated in more detail.

3.3 The alkalinity transfer efficiency and CO₂ sequestration efficiency

The final step in the mERW process represents the transfer of alkalinity to the surface water and subsequent equilibration of CO_2 at the air-sea interface (Fig. 2a). The upward transfer of alkalinity to the sea surface occurs on a time scale of weeks depending on the water depth (He and Tyka, 2023; Jones et al., 2014), and the air-sea CO_2 exchangetakes place on a time scale of months up to a year, with longer timescales associated with deep mixed layers (He and Tyka, 2023; Jones et al., 2014). The proportion of alkalinity that reaches the surface water and equilibrates with the atmosphere is given by the alkalinity transfer efficiency η_{A_T}, a time-dependent factor that varies between 0 and 1. Based on model simulations, He and Tyka (2023) demonstrated that many coastal systems reach η_{A_T} values of 0.8–1 after 3–4 years, but that lower η_{A_T} values (~0.44–0.75) were associated with coastlines that display deep-water formation. The η_{A_T} factor demonstrates the importance of deploying mERW in areas with sufficient water mixing so that bottom water alkalinity can reach the surface to get sufficient contact with the atmosphere. As most mERW modelling studies assume (near) instantaneous alkalinity release into the surface water (e.g., Feng et al., 2017; Hauck et al., 2016; Köhler et al., 2013), the alkalinity transfer efficiency and its effect on the CO_2 sequestration should be accounted for in further studies.

The amount of CO_2 that will subsequently be captured as the surface water and atmosphere equilibrate is given by the CO_2 sequestration efficiency ρ_{CO_2}, which is a thermodynamic quantity defined as (Zeebe and Wolf-Gladrow, 2001):

$$\rho_{CO_2} = \left(\frac{\partial DIC}{\partial A_T} \right)_{f_{CO_2}} \tag{13}$$

This partial derivative represents the change in the concentration of DIC upon the addition of one mole of alkalinity (A_T) to the seawater, evaluated at a constant fugacity (or partial pressure) of CO_2 (f_{CO_2}) (Wolf-Gladrow et al., 2007; Bertagni and Porporato, 2022). The value of ρ_{CO_2} can be calculated using dedicated software packages for seawater carbonate chemistry like AquaEnv (Hofmann et al., 2009) or CO2sys (Xu et al., 2017).

The magnitude of ρ_{CO_2} depends on the local seawater chemistry, temperature, and salinity, causing ρ_{CO_2} to vary between different coastal systems (Middelburg et al., 2020; Bertagni and Porporato, 2022). Across the global ocean, ρ_{CO_2} ranges from

770   ~0.75–0.95 with an average value of 0.84 (Bertagni and Porporato, 2022; Schulz et al., 2023). Figure 6a displays the predicted DIC as a function of alkalinity for a set of endmember conditions for salinity and temperature relevant to coastal systems. This graph illustrates the key mechanism underlying OAE: an increase in the alkalinity of seawater leads to an increase in DIC after equilibration with the atmosphere. The slope of the lines depict ρ_{CO_2} (Bertagni and Porporato, 2022; Schulz et al., 2023), which depends on temperature, salinity, and local seawater chemistry. Colder and less saline waters can store more CO_2 (Zeebe

775   and Wolf-Gladrow, 2001) and are characterized by a higher ρ_{CO_2} (Fig. 6a). Figure 6b–d illustrate the impact of local seawater chemistry (i.e., as specified by pH and f_{CO_2}), temperature, and salinity on ρ_{CO_2}. As a reference condition, we use pH = 8.07 (all pH values presented are on the total pH scale), temperature = 15°C, salinity = 35, and current CO_2 levels (f_{CO_2} = 420 ppm).

    The surface ocean pH between 60°N to 60°S varies between 8.0 and 8.25, with a global average of 8.07 ± 0.02 (Jiang et al.,

780   2019). In coastal areas, riverine input can cause larger variations in the pH, since the pH of rivers typically ranges between 6 and 8 (Mackenzie and Lerman, 2006). As shown in Fig. 6b, the pH exerts a strong influence on ρ_{CO_2} when moving across the entire pH scale from 4 to 12. At pH <5, ρ_{CO_2} effectively becomes zero since the addition of alkalinity here leads to a consumption of H^+ rather than the production of HCO_3^- or CO_3^{2-}, and hence there is no scavenging of CO_2 (Bertagni and Porporato, 2022; Hofmann et al., 2008). At higher pH, ρ_{CO_2} increases to a maximum value of 0.97 at pH = 6.7, before

785   decreasing again beyond pH ~8 and stabilizing at $\rho_{CO_2} \approx 0.5$ at pH > 10. Note that the value of $\rho_{CO_2} = 1$ is never reached in seawater due to the presence of the borate buffer (Bertagni and Porporato, 2022). When considering the typical current ocean seawater pH range of 8.0–8.25, the ρ_{CO_2} variation is minimal with values of 0.83-0.88 (Fig. 6b).
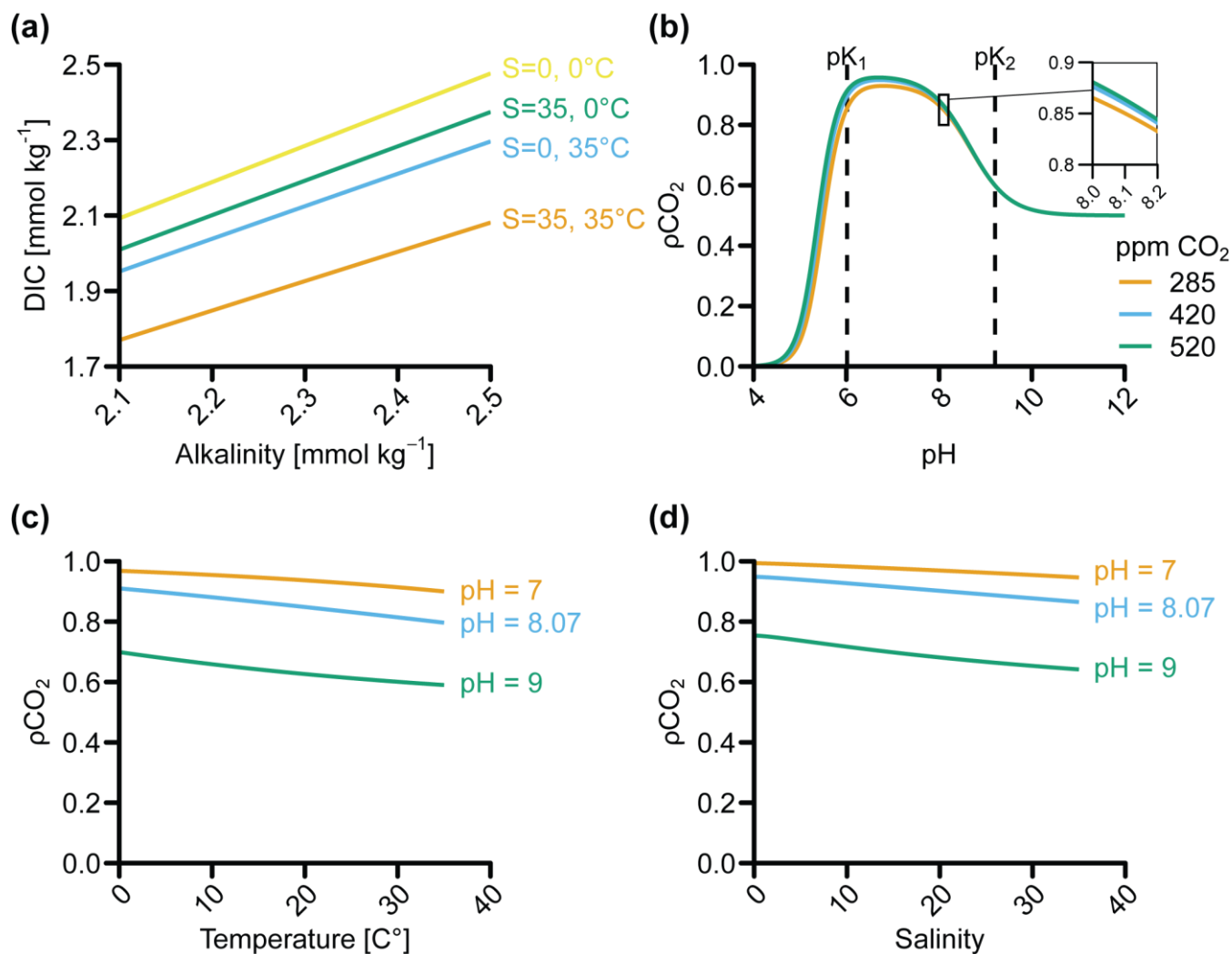
Figure 6. The CO₂ sequestration efficiency (ρ_{CO_2}) as a function of environmental parameters (unless otherwise stated pH = 8.07, temperature = 15 °C, salinity = 35, f_{CO_2} = 420 ppm). (a) Predicted DIC as a function of alkalinity for a set of endmember temperature and salinity values. (b) ρ_{CO_2} as a function of pH at different levels of atmospheric CO₂ (constant temperature and salinity), with pK values from Lueker et al. (2000). Typical seawater pH is shown in magnification. (c) ρ_{CO_2} as a function of temperature at different pH levels (constant salinity and f_{CO_2}).

Temperature and salinity influence ρ_{CO_2} through the stoichiometric equilibrium constants (K^*) of the carbonate system: ρ_{CO_2} decreases with increasing temperature (Fig. 6c) and increasing salinity (Fig. 6d). The temperature effect is in large part due to the presence of a borate buffer in seawater, which also contributes to alkalinity. An increase in temperature decreases the solubility of CO₂ without affecting the borate concentration, leading to a decreasing ratio between DIC and borate (Bertagni and Porporato, 2022). Across the ocean, the temperature varies between 0 and 35°C (Sarmiento and Gruber, 2006), which results in a ρ_{CO_2} range from 0.80 to 0.91 (Fig. 6c).

800 The effect of salinity on ρ_{CO_2} is driven by ion activity. When the salinity (and hence the number of ions in solution) increases, the ion activity decreases. Since the activities of different ions are not affected by the same magnitude, the ratio of their activity coefficients changes. For the carbonate system, the activity coefficient of the bivalent CO_3^{2-} decreases more rapidly with increasing salinity than those of the monovalent ions HCO_3^- and H^+. A decrease in salinity thus shifts the entire ρ_{CO_2} curve to the left (Fig. 6a). The impact of salinity on ρ_{CO_2} in the open ocean is minimal, as the variation in surface salinity is in the

805 range 33–37 (Sarmiento and Gruber, 2006), giving a ρ_{CO_2} difference of <0.01 (Fig. 6d). In estuaries, however, the salinity can vary from 0–35, which implies a decrease in ρ_{CO_2} from 0.95 to 0.86.

The atmospheric CO_2 concentration also affects ρ_{CO_2}. When atmospheric CO_2 levels increase, more CO_2 moves into solution to maintain the equilibrium between water and air, as described by Le Chatelier's principle. An increase in the atmospheric CO_2 concentration of 100 ppm would increase ρ_{CO_2} by ~0.004.

810 In conclusion, ρ_{CO_2} is easily calculated from environmental parameters, and is maximized in systems with low temperature, pH, and salinity. However, the precise value for η_{A_T} is difficult to quantify, but likely equates to ~0.8–1 in well mixed shallow systems. It is paramount that mERW is applied in areas where alkalinity is not lost to the deep ocean (He and Tyka, 2023).

4 Conclusions and future outlook

CDR technologies are urgently required to meet the targets of the Paris Climate Agreement, and OAE through mERW is

815 considered a promising candidate (Meysman and Montserrat, 2017). A considerable advantage of mERW is the possibility of rapid deployment and scalability, as no new technologies need to be developed. Since mERW mimics the natural process of chemical rock weathering, its theoretical underpinnings are well understood: when fine-grained silicates are added to coastal sediment environments, they remain out of thermodynamic equilibrium and will dissolve, thus releasing alkalinity (Fig. 2a). Although mining efforts would have to be substantially expanded to supply olivine for mERW, potential dunite reserves are

820 relatively large, so resource availability does not appear to be a limiting factor. Furthermore, the deposition of olivine onto the seafloor is expected to increase the dissolution rate of olivine by exposing it to the benthic weathering engine: chemical weathering can be enhanced by wave-induced physical abrasion, removal of weathering products through advection and bioirrigation, and exposure to a lower pH (compared to the overlying water). Although initial studies are positive (Flipkens et al., 2023b), the efficiency of this benthic weathering engine under relevant natural conditions remains poorly quantified, and

825 so this is an important point of attention for future mERW studies.

Coastal environments are geochemically complex and heterogeneous, so the practical implementation of mERW requires consideration of many processes, some of which are still poorly constrained (e.g. the impact of saturation effects in the pore water in different types of coastal sediments). Moreover, the intrinsic geochemical difference between various types of coastal sediments (e.g. cohesive versus permeable versus bedload) has been given very little attention. In addition, much of our current

830 understanding of the efficiency of mERW is based on laboratory experiments in aqueous solutions water with high fluid-to-mineral ratios, and it is unknown to what extent these results can be extrapolated to natural mERW field sites. Here, we have

provided a systematic review of the parameters that determine the CO_2 sequestration rate of olivine-based mERW (Table 4) and have identified aspects that need consideration when applying ERW in coastal environments.

Table 4. Summary of predictability of each parameter needed to calculate the CO_2 sequestration rate from mERW (basis for classification in supplementary file 1.4).

Parameter	Symbol	Predictability
CO_2 sequestration efficiency	ρ_{CO_2}	High
Molar mass olivine	$M_{olivine}$	High
Mass fraction of inert minerals	x_{inert}	High
Alkalinity transfer efficiency	η_{A_T}	Moderate
Intrinsic olivine dissolution rate	k_d	Moderate
Specific surface area	A_{surf}	Moderate
Alkalinity production factor	γ_{A_T}	Low
Saturation factor	Ω	Low

Table 4 lists the key parameters that affect the dissolution of olivine and the associated CO_2 sequestration efficiency and provides an assessment of their current predictability (i.e. how well we can predict them for a given environment with current knowledge). The CO_2 sequestration efficiency $\left(\rho_{CO_2}\right)$, mass fraction of inert minerals (x_{inert}), and molar mass of olivine $\left(M_{olivine}\right)$ are classified as "highly predictable" as they can either be calculated from environmental data (ρ_{CO_2}) or can be accurately derived by chemical analysis of the source rock of olivine (x_{inert} and $M_{olivine}$). The alkalinity transfer efficiency $\left(\eta_{A_T}\right)$ can be estimated using coupled chemical-hydrodynamical models (e.g., Daewel and Schrum, 2013; He and Tyka, 2023), if such models are available at sufficient resolution for the application site. Furthermore, the prediction of the dissolution rate of olivine in actual coastal sediments is hampered by several uncertainties, and so the predictability of the associated parameters; the intrinsic olivine dissolution rate (k_d), and specific surface area (A_{surf}) are qualified as "moderate". The intrinsic olivine dissolution rate is well-studied in laboratory settings, but its actual value within actual marine sediments bears considerable uncertainty. Experiments with a particular focus on mERW are typically conducted in laboratory reactors with high fluid-to-sediment ratios. Little information on the intrinsic olivine dissolution rate within actual sediments is available, which makes it difficult to estimate for the three suggested mERW scenarios (bedload, permeable, and cohesive sediment applications). Therefore, attaining estimates of the intrinsic dissolution rate in different natural sediment settings should be a research priority. As pH is a critical parameter in determining the intrinsic dissolution rate, an improved understanding of pore water pH as a function of sediment type would be beneficial in assessing which application sites are promising for mERW. Furthermore, a more detailed and systematic monitoring of the specific surface area of the olivine grains seems adamant. The specific surface area and grain roughness are typically only measured or reported before the start of dissolution experiments;

measurements throughout (long-term) applications could give important information on how the reactive surface area changes during mERW application.

Another important parameter governing olivine dissolution is the saturation factor (Ω), for which the predictability is qualified as "low" due to the low amount of data currently available. The uncertainty relates to the residence time of the pore water, which is determined by an intricate interplay between the grain size and properties of the ambient sediment, the local hydrodynamics, and the benthic fauna community composition. It seems imperative to mERW that olivine is applied to well-flushed sediments so that alkalinity and weathering products do not accumulate (hence $\Omega \ll 1$).

Also, the predictability of the alkalinity production factor (γ_{A_T}) is qualified as "low". The formation of the clay minerals sepiolite and serpentine seems unlikely in coastal sediment conditions, however, the formation of clay mineral assemblages (iddingsite and smectites) has not been thoroughly addressed. The prevalence of carbonate precipitation reactions is uncertain. Initial studies suggest that carbonate precipitation would be limited and that the risk of runaway precipitation (in the sediment or water) during mERW is low since alkalinity is released slowly and is added to an extensive volume of water. However, a critical unknown is how mERW would impact natural carbonate dissolution within the sediment and whether the alkalinity generated via mERW is fully additive to the natural alkalinity generation (Bach, 2024).

Considering the factors in Table 4, the suitability of certain sites for application of mERW can be evaluated. The most ideal locations are areas that are warm or relatively acidic, as these factors contribute positively to the weathering rate of olivine through the intrinsic dissolution rate. For mERW, it is key that sediments are targeted where olivine dissolution products do not build up, to avoid secondary mineral formation or inhibition of natural alkalinity production. However, the balance between removal of dissolution products and sufficient build-up of acidity to enhance the olivine dissolution should be considered with regards to the water exchange rate. Additionally, it is important that the generated alkalinity is able to reach the surface water and equilibrate fully with the atmosphere, implying that coastal waters should be well-mixed and that olivine is not deployed in areas characterized by downwelling to the deep sea. Furthermore, olivine mines should be close to the coast to limit costly overland transport and avoid transport emissions (which negatively impacts the CO_2 sequestration efficiency).

Overall, we conclude that whilst studies show a clear potential for mERW as a CDR method, the approach is not ready for upscaling and commercial exploitation. Future experiments should focus on improved quantification of olivine dissolution rates as well as alkalinity release rates in actual sediment environments. There is hence a clear need for *in situ* field trials, which are essential to quantify how efficiently mERW performs as an OAE technology. Before field trials are launched, microcosm and mesocosm experiments with natural sediment are crucial to increase the predictability of mERW effects. Both alkalinity effluxes from the sediment as well as the chemical conditions in the pore water before and after the application of olivine should be monitored. Since the effect of mERW is expected to vary seasonally, measurements should have a sufficiently high temporal resolution to allow trends to be quantified for MRV. Olivine grains should further be recovered throughout experiments to verify olivine dissolution features, formation of passivating layers, and occurrence of secondary mineral reactions. Detailed evaluations of the ecotoxicological and environmental impacts of mERW are another prerequisite for field

trials. Accordingly, a critical next step for mERW is to determine the efficacy of CO_2 drawdown in real-life conditions and its impacts on the broader environment. Moreover, the outcome of these field experiments will determine MRV protocols, which need to be designed and agreed upon, so that mERW applications can proceed in a sustainable and economically feasible manner.

Author contribution

LG was responsible for formal analysis, data collection, visualization, and writing of the original draft. LG and FJRM were responsible for the conceptualization. FJRM conceived and supervised the study. LG and FJRM took the lead in writing with additional input from AH. All authors discussed the results and contributed to the final manuscript.

Competing interests

The authors declare that they have no conflict of interest.

Financial support

LG was supported by a PhD fellowship from the Research Foundation – Flanders (FWO) (project number 1S08321N). AH was supported by a junior postdoctoral fellowship from FWO (project nr 1241724N). FJRM was supported by the Strategic Basic Research (SBO) project from FWO (project nr S000619N). This research was financially supported by Team for the Planet (https://team-planet.com), a citizen community initiative dedicated to tackling the climate challenge (funding through a collaboration agreement with its Carbon Time subsidiary).

Acknowledgments

The authors thank Sebastiaan van de Velde and Gunter Flipkens for academic discussions, and Vincent Sluydts for his assistance with calculating the uncertainty for the intrinsic dissolution rate constant. Ivan Communod and Mathieu Helwig from Carbon Time are thanked for their support through Team for the Planet.

References

Ackerman, L., Jelínek, E., Medaris, G., Ježek, J., Siebel, W., and Strnad, L.: Geochemistry of Fe-rich peridotites and associated pyroxenites from Horní Bory, Bohemian Massif: Insights into subduction-related melt–rock reactions, Chem. Geol., 259, 152–167, https://doi.org/10.1016/j.chemgeo.2008.10.042, 2009.

Aller, R. C.: 8.11 - Sedimentary Diagenesis, Depositional Environments, and Benthic Fluxes, in: Treatise on Geochemistry
915 (Second Edition), edited by: Holland, H. D. and Turekian, K. K., Elsevier, Oxford, 293–334, https://doi.org/10.1016/B978-0-08-095975-7.00611-2, 2014.

Alt, J. C., Shanks, W. C., Crispini, L., Gaggero, L., Schwarzenbach, E. M., Früh-Green, G. L., and Bernasconi, S. M.: Uptake of carbon and sulfur during seafloor serpentinization and the effects of subduction metamorphism in Ligurian peridotites, Chem. Geol., 322–323, 268–277, https://doi.org/10.1016/j.chemgeo.2012.07.009, 2012.

920 Alt, J. C., Schwarzenbach, E. M., Früh-Green, G. L., Shanks, W. C., Bernasconi, S. M., Garrido, C. J., Crispini, L., Gaggero, L., Padrón-Navarta, J. A., and Marchesi, C.: The role of serpentinites in cycling of carbon and sulfur: Seafloor serpentinization and subduction metamorphism, Lithos, 178, 40–54, https://doi.org/10.1016/j.lithos.2012.12.006, 2013.

Archer, D., Eby, M., Brovkin, V., Ridgwell, A., Cao, L., Mikolajewicz, U., Caldeira, K., Matsumoto, K., Munhoven, G., Montenegro, A., and Tokos, K.: Atmospheric Lifetime of Fossil Fuel Carbon Dioxide, Annu. Rev. Earth Planet. Sci., 37, 117–
925 134, https://doi.org/10.1146/annurev.earth.031208.100206, 2009.

Bach, L. T.: The additionality problem of ocean alkalinity enhancement, Biogeosciences, 21, 261–277, https://doi.org/10.5194/bg-21-261-2024, 2024.

Bach, L. T., Gill, S. J., Rickaby, R. E. M., Gore, S., and Renforth, P.: CO2 Removal With Enhanced Weathering and Ocean Alkalinity Enhancement: Potential Risks and Co-benefits for Marine Pelagic Ecosystems, Front. Clim., 1, 2019.

930 Bailey, A.: Proceedings of the International Symposium on Water-Rock Interaction (eds. J. Cadek and T. Paces), in: Effects of temperature on the reaction of silicates with aqueous solutions in the low temperature range, Geological Survey Prague, Prague, 375–380, 1976.

Baker, I. and Haggerty, S. E.: The alteration of olivine in basaltic and associated lavas, Contrib. Mineral. Petrol., 16, 258–273, https://doi.org/10.1007/BF00371095, 1967.

935 Baldermann, A., Mavromatis, V., Frick, P. M., and Dietzel, M.: Effect of aqueous Si/Mg ratio and pH on the nucleation and growth of sepiolite at 25 °C, Geochim. Cosmochim. Acta, 227, 211–226, https://doi.org/10.1016/j.gca.2018.02.027, 2018.

Béarat, H., McKelvy, M. J., Chizmeshya, A. V. G., Gormley, D., Nunez, R., Carpenter, R. W., Squires, K., and Wolf, G. H.: Carbon Sequestration via Aqueous Olivine Mineral Carbonation: Role of Passivating Layer Formation, Environ. Sci. Technol., 40, 4802–4808, https://doi.org/10.1021/es0523340, 2006.

940 Beerling, D. J., Leake, J. R., Long, S. P., Scholes, J. D., Ton, J., Nelson, P. N., Bird, M., Kantzas, E., Taylor, L. L., Sarkar, B., Kelland, M., DeLucia, E., Kantola, I., Müller, C., Rau, G., and Hansen, J.: Farming with crops and rocks to address global climate, food and soil security, Nat. Plants, 4, 138–147, https://doi.org/10.1038/s41477-018-0108-y, 2018.

Berner, R. A.: Sedimentary pyrite formation: An update, Geochim. Cosmochim. Acta, 48, 605–615, https://doi.org/10.1016/0016-7037(84)90089-9, 1984.

945 Berner, R. A.: The Phanerozoic Carbon Cycle: CO2 and O2, 1st ed., Oxford University Press, USA, 2004.

Berner, R. A., Lasaga, A. C., and Garrels, R. M.: The carbonate-silicate geochemical cycle and its effect on atmospheric carbon dioxide over the past 100 million years, Am. J. Sci., 283, 641–683, https://doi.org/10.2475/ajs.283.7.641, 1983.

Bertagni, M. B. and Porporato, A.: The Carbon-Capture Efficiency of Natural Water Alkalinization: Implications For Enhanced weathering, Sci. Total Environ., 838, 156524, https://doi.org/10.1016/j.scitotenv.2022.156524, 2022.

950   Blum, A. and Lasaga, A.: Role of surface speciation in the low-temperature dissolution of minerals, Nature, 331, 431–433, https://doi.org/10.1038/331431a0, 1988.

Brantley, S. L. and Mellott, N. P.: Surface area and porosity of primary silicate minerals, Am. Mineral., 85, 1767–1783, https://doi.org/10.2138/am-2000-11-1220, 2000.

Brantley, S. L., Kubicki, J. D., and White, A. F. (Eds.): Kinetics of water-rock interaction, Springer Verlag, New York, 833
955   pp., 2008.

Brown, G. and Stephen, I.: A Structural study of iddingsite from New South Wales, Australia, Am. Mineral., 44, 251–260, 1959.

Brunauer, S., Emmett, P. H., and Teller, E.: Adsorption of Gases in Multimolecular Layers, J. Am. Chem. Soc., 60, 309–319, https://doi.org/10.1021/ja01269a023, 1938.

960   Bucher, K. and Grapes, R.: Metamorphism of Ultramafic Rocks, in: Petrogenesis of Metamorphic Rocks, edited by: Bucher, K. and Grapes, R., Springer, Berlin, Heidelberg, 191–224, https://doi.org/10.1007/978-3-540-74169-5_5, 2011.

Bullock, L. A., James, R. H., Matter, J., Renforth, P., and Teagle, D. A. H.: Global Carbon Dioxide Removal Potential of Waste Materials From Metal and Diamond Mining, Front. Clim., 0, https://doi.org/10.3389/fclim.2021.694175, 2021.

Cai, W.-J., Reimers, C. E., and Shaw, T.: Microelectrode studies of organic carbon degradation and calcite dissolution at a
965   California Continental rise site, Geochim. Cosmochim. Acta, 59, 497–511, https://doi.org/10.1016/0016-7037(95)00316-R, 1995.

Campbell, J. S., Foteinis, S., Furey, V., Hawrot, O., Pike, D., Aeschlimann, S., Maesano, C. N., Reginato, P. L., Goodwin, D. R., Looger, L. L., Boyden, E. S., and Renforth, P.: Geochemical Negative Emissions Technologies: Part I. Review, Front. Clim., 4, 2022.

970   Caserini, S., Pagano, D., Campo, F., Abbà, A., De Marco, S., Righi, D., Renforth, P., and Grosso, M.: Potential of Maritime Transport for Ocean Liming and Atmospheric CO2 Removal, Front. Clim., 3, 22, https://doi.org/10.3389/fclim.2021.575900, 2021.

Caserini, S., Storni, N., and Grosso, M.: The Availability of Limestone and Other Raw Materials for Ocean Alkalinity Enhancement, Glob. Biogeochem. Cycles, 36, e2021GB007246, https://doi.org/10.1029/2021GB007246, 2022.

975   Casey, W. H. and Sposito, G.: On the temperature dependence of mineral dissolution rates, Geochim. Cosmochim. Acta, 56, 3825–3830, https://doi.org/10.1016/0016-7037(92)90173-G, 1992.

Chen, Y. and Brantley, S. L.: Dissolution of forsteritic olivine at 65°C and 2, Chem. Geol., 165, 267–281, https://doi.org/10.1016/S0009-2541(99)00177-1, 2000.

Corner, A. and Pidgeon, N.: Like artificial trees? The effect of framing by natural analogy on public perceptions of
980   geoengineering, Clim. Change, 130, 425–438, https://doi.org/10.1007/s10584-014-1148-6, 2015.

Cornwall, W.: Climate crisis sparks effort to coax oceans to suck up carbon dioxide | Science | AAAS, Science, 2023.

Crundwell, F. K.: The mechanism of dissolution of forsterite, olivine and minerals of the orthosilicate group, Hydrometallurgy, 150, 68–82, https://doi.org/10.1016/j.hydromet.2014.09.006, 2014.

Cyronak, T., Albright, R., and Bach, L. T.: Field experiments in ocean alkalinity enhancement research, State Planet, 2-oae2023, 1–13, https://doi.org/10.5194/sp-2-oae2023-7-2023, 2023.

Daewel, U. and Schrum, C.: Simulating long-term dynamics of the coupled North Sea and Baltic Sea ecosystem with ECOSMO II: Model description and validation, J. Mar. Syst., 119–120, 30–49, https://doi.org/10.1016/j.jmarsys.2013.03.008, 2013.

Daval, D., Sissmann, O., Menguy, N., Saldi, G. D., Guyot, F., Martinez, I., Corvisier, J., Garcia, B., Machouk, I., Knauss, K. G., and Hellmann, R.: Influence of amorphous silica layer formation on the dissolution rate of olivine at 90°C and elevated pCO2, Chem. Geol., 284, 193–209, https://doi.org/10.1016/j.chemgeo.2011.02.021, 2011.

Deer, W. A., Howie, R. A., and Zussman, J.: Olivine, in: An Introduction to the Rock-Forming Minerals, 4–11, 2013.

Dehouck, E., Gaudin, A., Chevrier, V., and Mangold, N.: Mineralogical record of the redox conditions on early Mars, Icarus, 271, 67–75, https://doi.org/10.1016/j.icarus.2016.01.030, 2016.

Delvigne, J., Bisdom, E. B. A., Sleeman, J., and Stoops, G.: Olivines, their pseudomorphs and secondary products, 63, 1979.

Dickson, A. G.: pH scales and proton-transfer reactions in saline media such as sea water, Geochim. Cosmochim. Acta, 48, 2299–2308, https://doi.org/10.1016/0016-7037(84)90225-4, 1984.

Edwards, A. B.: The Formation of Iddingsite, Am. Mineral., 23, 277–281, 1938.

Eggleton, R. A.: Formation of Iddingsite Rims on Olivine: A Transmission Electron Microscope Study, Clays Clay Miner., 32, 1–11, https://doi.org/10.1346/CCMN.1984.0320101, 1984.

Eisaman, M. D., Geilert, S., Renforth, P., Bastianini, L., Campbell, J., Dale, A. W., Foteinis, S., Grasse, P., Hawrot, O., Löscher, C. R., Rau, G. H., and Rønning, J.: Assessing the technical aspects of ocean-alkalinity-enhancement approaches, State Planet, 2-oae2023, 1–29, https://doi.org/10.5194/sp-2-oae2023-3-2023, 2023.

Eriksson, E.: On the rate of dissolution of olivine in aqueous solutions, Vatten, 38, 409–415, 1982.

Feng, E. Y., Koeve, W., Keller, D. P., and Oschlies, A.: Model-Based Assessment of the CO2 Sequestration Potential of Coastal Ocean Alkalinization, Earths Future, 5, 1252–1266, https://doi.org/10.1002/2017EF000659, 2017.

Flipkens, G., Blust, R., and Town, R. M.: Deriving Nickel (Ni(II)) and Chromium (Cr(III)) Based Environmentally Safe Olivine Guidelines for Coastal Enhanced Silicate Weathering, Environ. Sci. Technol., https://doi.org/10.1021/acs.est.1c02974, 2021.

Flipkens, G., Horoba, K., Bostyn, K., Geerts, L. J. J., Town, R. M., and Blust, R.: Acute bioaccumulation and chronic toxicity of olivine in the marine amphipod Gammarus locusta, Aquat. Toxicol., 106662, https://doi.org/10.1016/j.aquatox.2023.106662, 2023a.

Flipkens, G., Fuhr, M., Fiers, G., Meysman, F. J. R., Town, R. M., and Blust, R.: Enhanced olivine dissolution in seawater through continuous grain collisions, Geochim. Cosmochim. Acta, 359, 84–99, https://doi.org/10.1016/j.gca.2023.09.002, 2023b.

Foteinis, S., Campbell, J. S., and Renforth, P.: Life Cycle Assessment of Coastal Enhanced Weathering for Carbon Dioxide Removal from Air, Environ. Sci. Technol., https://doi.org/10.1021/acs.est.2c08633, 2023.

Fuhr, M., Geilert, S., Schmidt, M., Liebetrau, V., Vogt, C., Ledwig, B., and Wallmann, K.: Kinetics of Olivine Weathering in Seawater: An Experimental Study, Front. Clim., 4, https://doi.org/10.3389/fclim.2022.831587, 2022.

1020   Fuhr, M., Wallmann, K., Dale, A. W., Diercks, I., Kalapurakkal, H. T., Schmidt, M., Sommer, S., Böhnke, S., Perner, M., and Geilert, S.: Disentangling artificial and natural benthic weathering in organic rich Baltic Sea sediments, Front. Clim., 5, https://doi.org/10.3389/fclim.2023.1245580, 2023.

Fuhr, M., Wallmann, K., Dale, A. W., Kalapurakkal, H. T., Schmidt, M., Sommer, S., Deusner, C., Spiegel, T., Kowalski, J., and Geilert, S.: Alkaline mineral addition to anoxic to hypoxic Baltic Sea sediments as a potentially efficient CO_2-removal
1025   technique, Front. Clim., 6, https://doi.org/10.3389/fclim.2024.1338556, 2024.

Fuss, S., Lamb, W. F., Callaghan, M. W., Hilaire, J., Creutzig, F., Amann, T., Beringer, T., Garcia, W. de O., Hartmann, J., Khanna, T., Luderer, G., Nemet, G. F., Rogelj, J., Smith, P., Vicente, J. L. V., Wilcox, J., Dominguez, M. del M. Z., and Minx, J. C.: Negative emissions—Part 2: Costs, potentials and side effects, Environ. Res. Lett., 13, 063002, https://doi.org/10.1088/1748-9326/aabf9f, 2018.

1030   Gaudin, A., Dehouck, E., Grauby, O., and Mangold, N.: Formation of clay minerals on Mars: Insights from long-term experimental weathering of olivine, Icarus, 311, 210–223, https://doi.org/10.1016/j.icarus.2018.01.029, 2018.

Gerrits, R., Pokharel, R., Breitenbach, R., Radnik, J., Feldmann, I., Schuessler, J. A., von Blanckenburg, F., Gorbushina, A. A., and Schott, J.: How the rock-inhabiting fungus *K. petricola* A95 enhances olivine dissolution through attachment, Geochim. Cosmochim. Acta, 282, 76–97, https://doi.org/10.1016/j.gca.2020.05.010, 2020.

1035   Gerrits, R., Wirth, R., Schreiber, A., Feldmann, I., Knabe, N., Schott, J., Benning, L. G., and Gorbushina, A. A.: High-resolution imaging of fungal biofilm-induced olivine weathering, Chem. Geol., 559, 119902, https://doi.org/10.1016/j.chemgeo.2020.119902, 2021.

Giammar, D. E., Bruant, R. G., and Peters, C. A.: Forsterite dissolution and magnesite precipitation at conditions relevant for deep saline aquifer storage and sequestration of carbon dioxide, Chem. Geol., 217, 257–276,
1040   https://doi.org/10.1016/j.chemgeo.2004.12.013, 2005.

Goff, F. and Lackner, K. S.: Carbon Dioxide Sequestering Using Ultramaf ic Rocks, Environ. Geosci., 5, 89–102, https://doi.org/10.1046/j.1526-0984.1998.08014.x, 1998.

Goff, F., Guthrie, G., Lipin, B., Fite, M., Chipera, S., Counce, D., Kluk, E., and Ziock, H.: Evaluation of ultramafic deposits in the Eastern United States and Puerto Rico as sources of magnesium for carbon dioxide sequestration, Los Alamos National
1045   Lab. (LANL), Los Alamos, NM (United States), https://doi.org/10.2172/754045, 2000.

Golubev, S. V., Pokrovsky, O. S., and Schott, J.: Experimental determination of the effect of dissolved CO_2 on the dissolution kinetics of Mg and Ca silicates at 25 °C, Chem. Geol., 217, 227–238, https://doi.org/10.1016/j.chemgeo.2004.12.011, 2005.

Grandstaff, D. E.: Changes in surface area and morphology and the mechanism of forsterite dissolution, Geochim. Cosmochim. Acta, 42, 1899–1901, https://doi.org/10.1016/0016-7037(78)90245-4, 1978.

1050   Grandstaff, D. E.: The dissolution rate of forsteritic olivine from Hawaiian beach sand, in: Rates of Chemical Weathering of Rocks and Minerals, edited by: Colman, S. M. and Dethier, D. P., Academic Press, 41–57, 1986.

Griffioen, J.: Enhanced weathering of olivine in seawater: The efficiency as revealed by thermodynamic scenario analysis, Sci. Total Environ., 575, 536–544, https://doi.org/10.1016/j.scitotenv.2016.09.008, 2017.

Hänchen, M., Prigiobbe, V., Storti, G., Seward, T. M., and Mazzotti, M.: Dissolution kinetics of fosteritic olivine at 90–150°C including effects of the presence of CO2, Geochim. Cosmochim. Acta, 70, 4403–4416, https://doi.org/10.1016/j.gca.2006.06.1560, 2006.

Hänchen, M., Krevor, S., Mazzotti, M., and Lackner, K. S.: Validation of a population balance model for olivine dissolution, Chem. Eng. Sci., 62, 6412–6422, https://doi.org/10.1016/j.ces.2007.07.065, 2007.

Hangx, S. J. T. and Spiers, C. J.: Coastal spreading of olivine to control atmospheric CO2 concentrations: A critical analysis of viability, Int. J. Greenh. Gas Control, 3, 757–767, https://doi.org/10.1016/j.ijggc.2009.07.001, 2009.

Harben, P. W. and Smith, C., Jr.: Olivine, in: Industrial minerals & rocks: commodities, markets, and uses, edited by: Kogel, J. E., Trivedi, N. C., Barker, J. M., and Krukowski, S. T., SME, Littleton, Colo., 679–683, 2006.

Hartmann, J., West, A. J., Renforth, P., Köhler, P., Rocha, C. L. D. L., Wolf-Gladrow, D. A., Dürr, H. H., and Scheffran, J.: Enhanced chemical weathering as a geoengineering strategy to reduce atmospheric carbon dioxide, supply nutrients, and mitigate ocean acidification, Rev. Geophys., 51, 113–149, https://doi.org/10.1002/rog.20004, 2013.

Hartmann, J., Suitner, N., Lim, C., Schneider, J., Marín-Samper, L., Arístegui, J., Renforth, P., Taucher, J., and Riebesell, U.: Stability of alkalinity in Ocean Alkalinity Enhancement (OAE) approaches – consequences for durability of CO_2 storage, Biogeosciences Discuss., 1–29, https://doi.org/10.5194/bg-2022-126, 2022.

Hartmann, J., Suitner, N., Lim, C., Schneider, J., Marín-Samper, L., Arístegui, J., Renforth, P., Taucher, J., and Riebesell, U.: Stability of alkalinity in ocean alkalinity enhancement (OAE) approaches – consequences for durability of CO_2 storage, Biogeosciences, 20, 781–802, https://doi.org/10.5194/bg-20-781-2023, 2023.

Harvey, L. D. D.: Mitigating the atmospheric CO2 increase and ocean acidification by adding limestone powder to upwelling regions, J. Geophys. Res. Oceans, 113, https://doi.org/10.1029/2007JC004373, 2008.

Hauck, J., Köhler, P., Wolf-Gladrow, D., and Völker, C.: Iron fertilisation and century-scale effects of open ocean dissolution of olivine in a simulated CO_2 removal experiment, Environ. Res. Lett., 11, 024007, https://doi.org/10.1088/1748-9326/11/2/024007, 2016.

Hausrath, E. M. and Brantley, S. L.: Basalt and olivine dissolution under cold, salty, and acidic conditions: What can we learn about recent aqueous weathering on Mars?, J. Geophys. Res. Planets, 115, https://doi.org/10.1029/2010JE003610, 2010.

He, J. and Tyka, M. D.: Limits and CO_2 equilibration of near-coast alkalinity enhancement, Biogeosciences, 20, 27–43, https://doi.org/10.5194/bg-20-27-2023, 2023.

Hellmann, R., Wirth, R., Daval, D., Barnes, J.-P., Penisson, J.-M., Tisserand, D., Epicier, T., Florin, B., and Hervig, R. L.: Unifying natural and laboratory chemical weathering with interfacial dissolution–reprecipitation: A study based on the nanometer-scale chemistry of fluid–silicate interfaces, Chem. Geol., 294–295, 203–216, https://doi.org/10.1016/j.chemgeo.2011.12.002, 2012.

Heřmanská, M., Voigt, M. J., Marieni, C., Declercq, J., and Oelkers, E. H.: A comprehensive and internally consistent mineral dissolution rate database: Part I: Primary silicate minerals and glasses, Chem. Geol., 597, 120807, https://doi.org/10.1016/j.chemgeo.2022.120807, 2022.

Hofmann, A. F., Meysman, F. J. R., Soetaert, K., and Middelburg, J. J.: A step-by-step procedure for pH model construction in aquatic systems, 25, https://doi.org/10.5194/bg-5-227-2008, 2008.

1090   Hofmann, A. F., Middelburg, J. J., Soetaert, K., and Meysman, F. J. R.: pH modelling in aquatic systems with time-variable acid-base dissociation constants applied to the turbid, tidal Scheldt estuary, Biogeosciences, 6, 1539–1561, https://doi.org/10.5194/bg-6-1539-2009, 2009.

Hu, X. and Cai, W.-J.: An assessment of ocean margin anaerobic processes on oceanic alkalinity budget, Glob. Biogeochem. Cycles, 25, https://doi.org/10.1029/2010GB003859, 2011.

1095   Huettel, M. and Rusch, A.: Advective particle transport into permeable sediments—evidence from experiments in an intertidal sandflat, Limnol. Oceanogr., 45, 525–533, https://doi.org/10.4319/lo.2000.45.3.0525, 2000.

IPCC: Climate Change 2023: Synthesis Report. Contribution of Working Groups I, II and III to the Sixth Assessment Report of the Intergovernmental Panel on Climate Change, edited by: Lee, H. and J. Romero, , https://doi.org/10.59327/IPCC/AR6-9789291691647.001, 2023.

1100   Isson, T. T. and Planavsky, N. J.: Reverse weathering as a long-term stabilizer of marine pH and planetary climate, Nature, 560, 471–475, https://doi.org/10.1038/s41586-018-0408-4, 2018.

Jiang, L.-Q., Carter, B. R., Feely, R. A., Lauvset, S. K., and Olsen, A.: Surface ocean pH and buffer capacity: past, present and future, Sci. Rep., 9, 18624, https://doi.org/10.1038/s41598-019-55039-4, 2019.

Johnson, K. S., Coale, K. H., and Jannasch, H. W.: Analytical chemistry and oceanography, Anal. Chem., 64, 1065A-1075A, 1105   https://doi.org/10.1021/ac00046a001, 1992.

Johnson, N. C., Thomas, B., Maher, K., Rosenbauer, R. J., Bird, D., and Brown, G. E.: Olivine dissolution and carbonation under conditions relevant for in situ carbon storage, Chem. Geol., 373, 93–105, https://doi.org/10.1016/j.chemgeo.2014.02.026, 2014.

Jones, D. C., Ito, T., Takano, Y., and Hsu, W.-C.: Spatial and seasonal variability of the air-sea equilibration timescale of 1110   carbon dioxide, Glob. Biogeochem. Cycles, 28, 1163–1178, https://doi.org/10.1002/2014GB004813, 2014.

Keefner, J. W., Mackwell, S. J., Kohlstedt, D. L., and Heidelbach, F.: Dependence of dislocation creep of dunite on oxygen fugacity: Implications for viscosity variations in Earth's mantle, J. Geophys. Res. Solid Earth, 116, https://doi.org/10.1029/2010JB007748, 2011.

Klein, C., Hurlbut, C. S., and Dana, J. D.: Systematic descriptions of rock-forming silicates, in: The 22nd edition of the manual 1115   of mineral science: (after James D. Dana), J. Wiley, New York, 490–563, 2002.

Köhler, P., Hartmann, J., and Wolf-Gladrow, D. A.: Geoengineering potential of artificially enhanced silicate weathering of olivine, Proc. Natl. Acad. Sci., 107, 20228–20233, https://doi.org/10.1073/pnas.1000545107, 2010.

Köhler, P., Abrams, J. F., Völker, C., Hauck, J., and Wolf-Gladrow, D. A.: Geoengineering impact of open ocean dissolution of olivine on atmospheric CO2, surface ocean pH and marine biology, Environ. Res. Lett., 8, 014009, 1120   https://doi.org/10.1088/1748-9326/8/1/014009, 2013.

Kramer, D. A.: Magnesium Minerals and Compounds, in: Industrial minerals & rocks: commodities, markets, and uses, edited by: Kogel, J. E., Trivedi, N. C., Barker, J. M., and Krukowski, S. T., SME, Littleton, Colo., 2006.

Kremer, D., Etzold, S., Boldt, J., Blaum, P., Hahn, K. M., Wotruba, H., and Telle, R.: Geological Mapping and Characterization of Possible Primary Input Materials for the Mineral Sequestration of Carbon Dioxide in Europe, Minerals, 9, 485, 1125   https://doi.org/10.3390/min9080485, 2019.

Kristensen, E.: Impact of polychaetes (Nereis spp. and Arenicola marina) on carbon biogeochemistry in coastal marine sediments†, Geochem. Trans., 2, 92, https://doi.org/10.1186/1467-4866-2-92, 2001.

Lackner, K. S.: Carbonate Chemistry for Sequestering Fossil Carbon, Annu. Rev. Energy Environ., 27, 193–232, https://doi.org/10.1146/annurev.energy.27.122001.083433, 2002.

1130 Lasaga, A. C., Soler, J. M., Ganor, J., Burch, T. E., and Nagy, K. L.: Chemical weathering rate laws and global geochemical cycles, Geochim. Cosmochim. Acta, 58, 2361–2386, https://doi.org/10.1016/0016-7037(94)90016-7, 1994.

Le Hir, P., Cayocca, F., and Waeles, B.: Dynamics of sand and mud mixtures: A multiprocess-based modelling strategy, Cont. Shelf Res., 31, S135–S149, https://doi.org/10.1016/j.csr.2010.12.009, 2011.

Le Maitre, R. W., Streckeisen, A., Zanettin, B., Le Bas, M. J., Bonin, B., and Bateman, P. (Eds.): Igneous Rocks: A
1135 Classification and Glossary of Terms: Recommendations of the International Union of Geological Sciences Subcommission on the Systematics of Igneous Rocks, 2nd ed., Cambridge University Press, Cambridge, https://doi.org/10.1017/CBO9780511535581, 2002.

Li, C., Liu, X., Li, Y., Jiang, Y., Guo, X., Hutchins, D. A., Ma, J., Lin, X., and Dai, M.: The interactions between olivine dissolution and phytoplankton in seawater: Potential implications for ocean alkalinization, Sci. Total Environ., 912, 168571,
1140 https://doi.org/10.1016/j.scitotenv.2023.168571, 2024.

Lin, C. Y., Turchyn, A. V., Krylov, A., and Antler, G.: The microbially driven formation of siderite in salt marsh sediments, Geobiology, 18, 207–224, https://doi.org/10.1111/gbi.12371, 2020.

Luce, R. W., Bartlett, R. W., and Parks, G. A.: Dissolution kinetics of magnesium silicates, Geochim. Cosmochim. Acta, 36, 35–50, https://doi.org/10.1016/0016-7037(72)90119-6, 1972.

1145 Lueker, T. J., Dickson, A. G., and Keeling, C. D.: Ocean pCO2 calculated from dissolved inorganic carbon, alkalinity, and equations for K1 and K2: validation based on laboratory measurements of CO2 in gas and seawater at equilibrium, Mar. Chem., 70, 105–119, https://doi.org/10.1016/S0304-4203(00)00022-0, 2000.

Lunstrum, A., Van Den Berghe, M., Bian, X., John, S., Nealson, K., and West, A. J.: Bacterial use of siderophores increases olivine dissolution rates by nearly an order of magnitude | Geochemical Perspectives Letters, Geochem. Perspect. Lett., 25,
1150 https://doi.org/10.7185/geochemlet.2315, 2023.

Mackenzie, F. T. and Lerman, A.: Carbon Dioxide in Natural Waters, in: Carbon in the Geobiosphere — Earth's Outer Shell —, edited by: Mackenzie, F. T. and Lerman, A., Springer Netherlands, Dordrecht, 123–147, https://doi.org/10.1007/1-4020-4238-8_1, 2006.

Maher, K., Johnson, N. C., Jackson, A., Lammers, L. N., Torchinsky, A. B., Weaver, K. L., Bird, D. K., and Brown, G. E.: A
1155 spatially resolved surface kinetic model for forsterite dissolution, Geochim. Cosmochim. Acta, 174, 313–334, https://doi.org/10.1016/j.gca.2015.11.019, 2016.

Mével, C.: Serpentinization of abyssal peridotites at mid-ocean ridges, Comptes Rendus Geosci., 335, 825–852, https://doi.org/10.1016/j.crte.2003.08.006, 2003.

Meysman, F. J. R.: Cable Bacteria Take a New Breath Using Long-Distance Electricity, Trends Microbiol., 26, 411–422,
1160 https://doi.org/10.1016/j.tim.2017.10.011, 2018.

Meysman, F. J. R. and Montserrat, F.: Negative CO$_2$ emissions via enhanced silicate weathering in coastal environments, Biol. Lett., 13, 20160905, https://doi.org/10.1098/rsbl.2016.0905, 2017.

Meysman, F. J. R., Galaktionov, O. S., Cook, P. L. M., Janssen, F., Huettel, M., and Middelburg, J. J.: Quantifying biologically and physically induced flow and tracer dynamics in permeable sediments, Biogeosciences, 4, 627–646, https://doi.org/10.5194/bg-4-627-2007, 2007.

Meysman, F. J. R., Risgaard-Petersen, N., Malkin, S. Y., and Nielsen, L. P.: The geochemical fingerprint of microbial long-distance electron transport in the seafloor, Geochim. Cosmochim. Acta, 152, 122–142, https://doi.org/10.1016/j.gca.2014.12.014, 2015.

Middelburg, J. J., Soetaert, K., and Hagens, M.: Ocean Alkalinity, Buffering and Biogeochemical Processes, Rev. Geophys., 58, e2019RG000681, https://doi.org/10.1029/2019RG000681, 2020.

Milliman, J. D. and Droxler, A. W.: Neritic and pelagic carbonate sedimentation in the marine environment: ignorance is not bliss, Geol. Rundsch., 85, 496–504, https://doi.org/10.1007/BF02369004, 1996.

Minx, J. C., Lamb, W. F., Callaghan, M. W., Fuss, S., Hilaire, J., Creutzig, F., Amann, T., Beringer, T., Garcia, W. de O., Hartmann, J., Khanna, T., Lenzi, D., Luderer, G., Nemet, G. F., Rogelj, J., Smith, P., Vicente, J. L. V., Wilcox, J., and Dominguez, M. del M. Z.: Negative emissions—Part 1: Research landscape and synthesis, Environ. Res. Lett., 13, 063001, https://doi.org/10.1088/1748-9326/aabf9b, 2018.

Montserrat, F., Renforth, P., Hartmann, J., Leermakers, M., Knops, P., and Meysman, F. J. R.: Olivine Dissolution in Seawater: Implications for CO2 Sequestration through Enhanced Weathering in Coastal Environments, Environ. Sci. Technol., 51, 3960–3972, https://doi.org/10.1021/acs.est.6b05942, 2017.

Moosdorf, N., Renforth, P., and Hartmann, J.: Carbon Dioxide Efficiency of Terrestrial Enhanced Weathering, Environ. Sci. Technol., 48, 4809–4816, https://doi.org/10.1021/es4052022, 2014.

Moras, C. A., Bach, L. T., Cyronak, T., Joannes-Boyau, R., and Schulz, K. G.: Ocean alkalinity enhancement – avoiding runaway CaCO$_3$ precipitation during quick and hydrated lime dissolution, Biogeosciences, 19, 3537–3557, https://doi.org/10.5194/bg-19-3537-2022, 2022.

Moras, C. A., Joannes-Boyau, R., Bach, L. T., Cyronak, T., and Schulz, K. G.: Carbon dioxide removal efficiency of iron and steel slag in seawater via ocean alkalinity enhancement, Front. Clim., 6, https://doi.org/10.3389/fclim.2024.1396487, 2024.

Morse, J. W. and Mackenzie, F. T.: Geochemistry of Sedimentary Carbonates, Elsevier Science, 1990.

Morse, J. W., Arvidson, R. S., and Lüttge, A.: Calcium Carbonate Formation and Dissolution, Chem. Rev., 107, 342–381, https://doi.org/10.1021/cr050358j, 2007.

Mulders, J. J. P. A. and Oelkers, Eric. H.: An experimental study of sepiolite dissolution rates and mechanisms at 25 °C, Geochim. Cosmochim. Acta, 270, 296–312, https://doi.org/10.1016/j.gca.2019.11.026, 2020.

Mulders, J. J. P. A., Harrison, A. L., Christ, J., and Oelkers, E. H.: Non-stoichiometric dissolution of sepiolite, Energy Procedia, 146, 74–80, https://doi.org/10.1016/j.egypro.2018.07.011, 2018.

NASEM: Ocean Alkalinity Enhancement, in: A Research Strategy for Ocean-based Carbon Dioxide Removal and Sequestration, National Academies Press (US), Washington (DC), https://doi.org/10.17226/26278, 2022.

Neubeck, A., Duc, N. T., Bastviken, D., Crill, P., and Holm, N. G.: Formation of H2 and CH4 by weathering of olivine at temperatures between 30 and 70°C, Geochem. Trans., 12, 6, https://doi.org/10.1186/1467-4866-12-6, 2011.

Niles, P. B., Michalski, J., Ming, D. W., and Golden, D. C.: Elevated olivine weathering rates and sulfate formation at cryogenic temperatures on Mars, Nat. Commun., 8, 998, https://doi.org/10.1038/s41467-017-01227-7, 2017.

1200   Oelkers, E. H.: An experimental study of forsterite dissolution rates as a function of temperature and aqueous Mg and Si concentrations, Chem. Geol., 175, 485–494, https://doi.org/10.1016/S0009-2541(00)00352-1, 2001a.

Oelkers, E. H.: General kinetic description of multioxide silicate mineral and glass dissolution, Geochim. Cosmochim. Acta, 65, 3703–3719, https://doi.org/10.1016/S0016-7037(01)00710-4, 2001b.

Oelkers, E. H., Declercq, J., Saldi, G. D., Gislason, S. R., and Schott, J.: Olivine dissolution rates: A critical review, Chem.
1205   Geol., 500, 1–19, https://doi.org/10.1016/j.chemgeo.2018.10.008, 2018.

Olsen, A. A.: Forsterite Dissolution Kinetics: Applications and Implications for Chemical Weathering, 2007.

Olsen, A. A. and Donald Rimstidt, J.: Oxalate-promoted forsterite dissolution at low pH, Geochim. Cosmochim. Acta, 72, 1758–1766, https://doi.org/10.1016/j.gca.2007.12.026, 2008.

Olsen, A. A., Hausrath, E. M., and Rimstidt, J. D.: Forsterite dissolution rates in Mg-sulfate-rich Mars-analog brines and
1210   implications of the aqueous history of Mars, J. Geophys. Res. Planets, 120, 388–400, https://doi.org/10.1002/2014JE004664, 2015.

Orlando, A., Borrini, D., and Marini, L.: Dissolution and carbonation of a serpentinite: Inferences from acid attack and high P–T experiments performed in aqueous solutions at variable salinity, Appl. Geochem., 26, 1569–1583, https://doi.org/10.1016/j.apgeochem.2011.06.023, 2011.

1215   Ouillon, S.: Why and How Do We Study Sediment Transport? Focus on Coastal Zones and Ongoing Methods, Water, 10, 390, https://doi.org/10.3390/w10040390, 2018.

Palandri, J. L. and Kharaka, Y. K.: A Compilation of Rate Parameters of Water-Mineral Interaction Kinetics for Application to Geochemical Modeling, Geological survey Menlo Park California, 2004.

te Pas, E. E. E. M., Hagens, M., and Comans, R. N. J.: Assessment of the enhanced weathering potential of different silicate
1220   minerals to improve soil quality and sequester CO2, Front. Clim., 4, https://doi.org/10.3389/fclim.2022.954064, 2023.

Pfeffer, C., Larsen, S., Song, J., Dong, M., Besenbacher, F., Meyer, R. L., Kjeldsen, K. U., Schreiber, L., Gorby, Y. A., El-Naggar, M. Y., Leung, K. M., Schramm, A., Risgaard-Petersen, N., and Nielsen, L. P.: Filamentous bacteria transport electrons over centimetre distances, Nature, 491, 218–221, https://doi.org/10.1038/nature11586, 2012.

Pfeifer, K., Hensen, C., Adler, M., Wenzhfer, F., Weber, B., and Schulz, H. D.: Modeling of subsurface calcite dissolution,
1225   including the respiration and reoxidation processes of marine sediments in the region of equatorial upwelling off Gabon, Geochim. Cosmochim. Acta, 66, 4247–4259, https://doi.org/10.1016/S0016-7037(02)01073-6, 2002.

Pokrovsky, O. S. and Schott, J.: Kinetics and mechanism of forsterite dissolution at 25°C and pH from 1 to 12, Geochim. Cosmochim. Acta, 64, 3313–3325, https://doi.org/10.1016/S0016-7037(00)00434-8, 2000.

Pokrovsky, O. S. and Schott, J.: Experimental study of brucite dissolution and precipitation in aqueous solutions: surface speciation and chemical affinity control, Geochim. Cosmochim. Acta, 68, 31–45, https://doi.org/10.1016/S0016-7037(03)00238-2, 2004.

Prigiobbe, V., Costa, G., Baciocchi, R., Hänchen, M., and Mazzotti, M.: The effect of CO2 and salinity on olivine dissolution kinetics at 120°C, Chem. Eng. Sci., 64, 3510–3515, https://doi.org/10.1016/j.ces.2009.04.035, 2009.

Rao, A. M. F., Polerecky, L., Ionescu, D., Meysman, F. J. R., and de Beer, D.: The influence of pore-water advection, benthic photosynthesis, and respiration on calcium carbonate dynamics in reef sands, Limnol. Oceanogr., 57, 809–825, https://doi.org/10.4319/lo.2012.57.3.0809, 2012.

Rao, A. M. F., Malkin, S. Y., Montserrat, F., and Meysman, F. J. R.: Alkalinity production in intertidal sands intensified by lugworm bioirrigation, Estuar. Coast. Shelf Sci., 148, 36–47, https://doi.org/10.1016/j.ecss.2014.06.006, 2014.

Rau, G. H.: Electrochemical Splitting of Calcium Carbonate to Increase Solution Alkalinity: Implications for Mitigation of Carbon Dioxide and Ocean Acidity, Environ. Sci. Technol., 42, 8935–8940, https://doi.org/10.1021/es800366q, 2008.

Rau, G. H., Willauer, H. D., and Ren, Z. J.: The global potential for converting renewable electricity to negative-CO2-emissions hydrogen, Nat. Clim. Change, 8, 621–625, https://doi.org/10.1038/s41558-018-0203-0, 2018.

Rehfeldt, T., Jacob, D. E., Carlson, R. W., and Foley, S. F.: Fe-rich Dunite Xenoliths from South African Kimberlites: Cumulates from Karoo Flood Basalts, J. Petrol., 48, 1387–1409, https://doi.org/10.1093/petrology/egm023, 2007.

Renforth, P.: The potential of enhanced weathering in the UK, Int. J. Greenh. Gas Control, 10, 229–243, https://doi.org/10.1016/j.ijggc.2012.06.011, 2012.

Renforth, P.: The negative emission potential of alkaline materials, Nat. Commun., 10, 1401, https://doi.org/10.1038/s41467-019-09475-5, 2019.

Renforth, P. and Henderson, G.: Assessing ocean alkalinity for carbon sequestration, Rev. Geophys., 55, 636–674, https://doi.org/10.1002/2016RG000533, 2017.

Renforth, P., Jenkins, B. G., and Kruger, T.: Engineering challenges of ocean liming, Energy, 60, 442–452, https://doi.org/10.1016/j.energy.2013.08.006, 2013.

Riahi, K., Bertram, C., Huppmann, D., Rogelj, J., Bosetti, V., Cabardos, A.-M., Deppermann, A., Drouet, L., Frank, S., Fricko, O., Fujimori, S., Harmsen, M., Hasegawa, T., Krey, V., Luderer, G., Paroussos, L., Schaeffer, R., Weitzel, M., van der Zwaan, B., Vrontisi, Z., Longa, F. D., Després, J., Fosse, F., Fragkiadakis, K., Gusti, M., Humpenöder, F., Keramidas, K., Kishimoto, P., Kriegler, E., Meinshausen, M., Nogueira, L. P., Oshiro, K., Popp, A., Rochedo, P. R. R., Ünlü, G., van Ruijven, B., Takakura, J., Tavoni, M., van Vuuren, D., and Zakeri, B.: Cost and attainability of meeting stringent climate targets without overshoot, Nat. Clim. Change, 11, 1063–1069, https://doi.org/10.1038/s41558-021-01215-2, 2021.

Riebesell, U., Basso, D., Geilert, S., Dale, A. W., and Kreuzburg, M.: Mesocosm experiments in ocean alkalinity enhancement research, State Planet, 2-oae2023, 1–14, https://doi.org/10.5194/sp-2-oae2023-6-2023, 2023.

Rigopoulos, I., Harrison, A. L., Delimitis, A., Ioannou, I., Efstathiou, A. M., Kyratsi, T., and Oelkers, E. H.: Carbon sequestration via enhanced weathering of peridotites and basalts in seawater, Appl. Geochem., 91, 197–207, https://doi.org/10.1016/j.apgeochem.2017.11.001, 2018.

Rimstidt, J. D., Brantley, S. L., and Olsen, A. A.: Systematic review of forsterite dissolution rate data, Geochim. Cosmochim. Acta, 99, 159–178, https://doi.org/10.1016/j.gca.2012.09.019, 2012.

Robinson, S. M., Santini, K., and Moroney, J.: Wollastonite, in: Industrial minerals & rocks: commodities, markets, and uses, edited by: Kogel, J. E., Trivedi, N. C., Barker, J. M., and Krukowski, S. T., SME, Littleton, Colo., 1027–1037, 2006.

Rockström, J., Gaffney, O., Rogelj, J., Meinshausen, M., Nakicenovic, N., and Schellnhuber, H. J.: A roadmap for rapid decarbonization, Science, 355, 1269–1271, https://doi.org/10.1126/science.aah3443, 2017.

Rosso, J. J. and Rimstidt, J. D.: A high resolution study of forsterite dissolution rates, Geochim. Cosmochim. Acta, 64, 797–811, https://doi.org/10.1016/S0016-7037(99)00354-3, 2000.

Saldi, G. D., Jordan, G., Schott, J., and Oelkers, E. H.: Magnesite growth rates as a function of temperature and saturation state, Geochim. Cosmochim. Acta, 73, 5646–5657, https://doi.org/10.1016/j.gca.2009.06.035, 2009.

Sanderson, B. M., O'Neill, B. C., and Tebaldi, C.: What would it take to achieve the Paris temperature targets?, Geophys. Res. Lett., 43, 7133–7142, https://doi.org/10.1002/2016GL069563, 2016.

Santos, R. M., Van Audenaerde, A., Chiang, Y. W., Iacobescu, R. I., Knops, P., and Van Gerven, T.: Nickel Extraction from Olivine: Effect of Carbonation Pre-Treatment, Metals, 5, 1620–1644, https://doi.org/10.3390/met5031620, 2015.

Sarmiento, J. L. and Gruber, N.: Ocean Biogeochemical Dynamics, Princeton University Press, https://doi.org/10.2307/j.ctt3fgxqx, 2006.

Schippers, A. and Jørgensen, B. B.: Biogeochemistry of pyrite and iron sulfide oxidation in marine sediments, Geochim. Cosmochim. Acta, 66, 85–92, https://doi.org/10.1016/S0016-7037(01)00745-1, 2002.

Schuiling, R. D. and Krijgsman, P.: Enhanced Weathering: An Effective and Cheap Tool to Sequester Co2, Clim. Change, 74, 349–354, https://doi.org/10.1007/s10584-005-3485-y, 2006.

Schulz, K. G., Bach, L. T., and Dickson, A. G.: Seawater carbonate chemistry considerations for ocean alkalinity enhancement research: theory, measurements, and calculations, State Planet, 2-oae2023, 1–14, https://doi.org/10.5194/sp-2-oae2023-2-2023, 2023.

Schwarzenbach, E. M., Früh-Green, G. L., Bernasconi, S. M., Alt, J. C., Shanks Iii, W. C., Gaggero, L., and Crispini, L.: Sulfur geochemistry of peridotite-hosted hydrothermal systems: Comparing the Ligurian ophiolites with oceanic serpentinites, Geochim. Cosmochim. Acta, 91, 283–305, https://doi.org/10.1016/j.gca.2012.05.021, 2012.

Sherman, G. D. and Uehara, G.: The Weathering of Olivine Basalt in Hawaii and its Pedogenic Significance, Soil Sci. Soc. Am. J., 20, 337–340, https://doi.org/10.2136/sssaj1956.03615995002000030011x, 1956.

Shirokova, L. S., Bénézeth, P., Pokrovsky, O. S., Gerard, E., Ménez, B., and Alfredsson, H.: Effect of the heterotrophic bacterium Pseudomonas reactans on olivine dissolution kinetics and implications for CO2 storage in basalts, Geochim. Cosmochim. Acta, 80, 30–50, https://doi.org/10.1016/j.gca.2011.11.046, 2012.

Siegel, D. I. and Pfannkuch, H. O.: Silicate mineral dissolution at pH 4 and near standard temperature and pressure, Geochim. Cosmochim. Acta, 48, 197–201, https://doi.org/10.1016/0016-7037(84)90362-4, 1984.

Silburn, B., Kröger, S., Parker, E. R., Sivyer, D. B., Hicks, N., Powell, C. F., Johnson, M., and Greenwood, N.: Benthic pH gradients across a range of shelf sea sediment types linked to sediment characteristics and seasonal variability, Biogeochemistry, 135, 69–88, https://doi.org/10.1007/s10533-017-0323-z, 2017.

1300   Simandl, G. J., Paradis, S., and Irvine, M.: Brucite - Industrial Mineral with a Future, Geosci. Can., 2007.

Sissmann, O., Daval, D., Brunet, F., Guyot, F., Verlaguet, A., Pinquier, Y., Findling, N., and Martinez, I.: The deleterious effect of secondary phases on olivine carbonation yield: Insight from time-resolved aqueous-fluid sampling and FIB-TEM characterization, Chem. Geol., 357, 186–202, https://doi.org/10.1016/j.chemgeo.2013.08.031, 2013.

Smith, K. L., Milnes, A. R., and Eggleton, R. A.: Weathering of Basalt: Formation of Iddingsite, Clays Clay Miner., 35, 418–
1305   428, https://doi.org/10.1346/CCMN.1987.0350602, 1987.

Smith, P., Davis, S. J., Creutzig, F., Fuss, S., Minx, J., Gabrielle, B., Kato, E., Jackson, R. B., Cowie, A., Kriegler, E., van Vuuren, D. P., Rogelj, J., Ciais, P., Milne, J., Canadell, J. G., McCollum, D., Peters, G., Andrew, R., Krey, V., Shrestha, G., Friedlingstein, P., Gasser, T., Grübler, A., Heidug, W. K., Jonas, M., Jones, C. D., Kraxner, F., Littleton, E., Lowe, J., Moreira, J. R., Nakicenovic, N., Obersteiner, M., Patwardhan, A., Rogner, M., Rubin, E., Sharifi, A., Torvanger, A., Yamagata, Y.,
1310   Edmonds, J., and Yongsung, C.: Biophysical and economic limits to negative CO 2 emissions, Nat. Clim. Change, 6, 42–50, https://doi.org/10.1038/nclimate2870, 2016.

Strefler, J., Amann, T., Bauer, N., Kriegler, E., and Hartmann, J.: Potential and costs of carbon dioxide removal by enhanced weathering of rocks, Environ. Res. Lett., 13, 034010, https://doi.org/10.1088/1748-9326/aaa9c4, 2018.

Su, B., Chen, Y., Guo, S., and Liu, J.: Origins of orogenic dunites: Petrology, geochemistry, and implications, Gondwana Res.,
1315   29, 41–59, https://doi.org/10.1016/j.gr.2015.08.001, 2016.

Summers, C. A., Dahlin, D. C., Rush, G. E., O'Connor, W. K., and Gerdemann, S. J.: Grinding methods to enhance the reactivity of olivine, Min. Metall. Explor., 22, 140–144, https://doi.org/10.1007/BF03403128, 2005.

Sun, K. H. and Huggins, M. L.: Energy additivity in oxygen-containing crystals and glasses., J. Phys. Colloid Chem., 51, 438–
443, https://doi.org/10.1021/j150452a009, 1947.

1320   Sun, M.-S.: The Nature of Iddingsite in Some Basaltic Rocks of New Mexico*, Am. Mineral., 42, 525–533, 1957.

Terlouw, T., Bauer, C., Rosa, L., and Mazzotti, M.: Life cycle assessment of carbon dioxide removal technologies: a critical review, Energy Environ. Sci., 14, 1701–1721, https://doi.org/10.1039/D0EE03757E, 2021.

Tester, J. W., Worley, W. G., Robinson, B. A., Grigsby, C. O., and Feerer, J. L.: Correlating quartz dissolution kinetics in pure water from 25 to 625°C, Geochim. Cosmochim. Acta, 58, 2407–2420, https://doi.org/10.1016/0016-7037(94)90020-5, 1994.

1325   Torres, M. A., Dong, S., Nealson, K. H., and West, A. J.: The kinetics of siderophore-mediated olivine dissolution, Geobiology, 17, 401–416, https://doi.org/10.1111/gbi.12332, 2019.

Tosca, N. J. and Masterson, A. L.: Chemical controls on incipient Mg-silicate crystallization at 25°C: Implications for early and late diagenesis, Clay Miner., 49, 165–194, https://doi.org/10.1180/claymin.2014.049.2.03, 2014.

Turchyn, A. V., Bradbury, H. J., Walker, K., and Sun, X.: Controls on the Precipitation of Carbonate Minerals Within Marine
1330   Sediments, Front. Earth Sci., 9, https://doi.org/10.3389/feart.2021.618311, 2021.

UNFCCC: Paris Agreement to the United Nations Framework Convention on Climate Change, 2015.

USGS: Can oceans store more CO2 to help with climate change? | U.S. Geological Survey, USGS, 2023.

Van Herk, J., Pietersen, H. S., and Schuiling, R. D.: Neutralization of industrial waste acids with olivine — The dissolution of forsteritic olivine at 40–70°C, Chem. Geol., 76, 341–352, https://doi.org/10.1016/0009-2541(89)90102-2, 1989.

1335 Vandeginste, V., Lim, C., and Ji, Y.: Exploratory Review on Environmental Aspects of Enhanced Weathering as a Carbon Dioxide Removal Method, Minerals, 14, 75, https://doi.org/10.3390/min14010075, 2024.

Velbel, M. A.: Bond strength and the relative weathering rates of simple orthosilicates, Am. J. Sci., 299, 679–696, https://doi.org/10.2475/ajs.299.7-9.679, 1999.

Velbel, M. A.: Dissolution of olivine during natural weathering, Geochim. Cosmochim. Acta, 73, 6098–6113, 1340 https://doi.org/10.1016/j.gca.2009.07.024, 2009.

Vesta: North Sea Beach Annual Monitoring Report, 2023.

Volkenborn, N., Polerecky, L., Hedtkamp, S. I. C., van Beusekom, J. E. E., and de Beer, D.: Bioturbation and bioirrigation extend the open exchange regions in permeable sediments, Limnol. Oceanogr., 52, 1898–1909, https://doi.org/10.4319/lo.2007.52.5.1898, 2007.

1345 Wallmann, K., Aloisi, G., Haeckel, M., Tishchenko, P., Pavlova, G., Greinert, J., Kutterolf, S., and Eisenhauer, A.: Silicate weathering in anoxic marine sediments, Geochim. Cosmochim. Acta, 72, 2895–2918, https://doi.org/10.1016/j.gca.2008.03.026, 2008.

Wang, B., Gao, X., Song, J., Li, X., Yuan, H., Xie, L., Zhao, J., Xing, Q., and Qin, S.: Feasibility of increasing marine carbon storage through olivine addition, J. Environ. Chem. Eng., 11, 111221, https://doi.org/10.1016/j.jece.2023.111221, 2023.

1350 White, A. F. and Brantley, S. L. (Eds.): Chemical Weathering Rates of Silicate Minerals, De Gruyter, Berlin, Boston, https://doi.org/doi:10.1515/9781501509650, 1995.

Widdicombe, S., Spicer, J. I., and Kitidis, V.: Effects of ocean acidification on sediment fauna, in: Ocean Acidification, edited by: Gattuso, J.-P., Hansson, L., Gattuso, J.-P., and Hansson, L., Oxford University Press, Oxford, New York, 2011.

Wilshire, H. G.: Alteration of olivine and orthopyroxene in basic lavas and shallow intrusions, Am. Mineral., 43, 120–147, 1355 1958.

Wilson, M. J.: Weathering of the primary rock-forming minerals: processes, products and rates, Clay Miner., 39, 233–266, https://doi.org/10.1180/0009855043930133, 2004.

Wogelius, R. A. and Walther, J. V.: Olivine dissolution at 25°C: Effects of pH, CO2, and organic acids, Geochim. Cosmochim. Acta, 55, 943–954, https://doi.org/10.1016/0016-7037(91)90153-V, 1991.

1360 Wolf-Gladrow, D. A., Zeebe, R. E., Klaas, C., Körtzinger, A., and Dickson, A. G.: Total alkalinity: The explicit conservative expression and its application to biogeochemical processes, Mar. Chem., 106, 287–300, https://doi.org/10.1016/j.marchem.2007.01.006, 2007.

Wollast, R., Mackenzie, F. T., and Bricker, O. P.: Experimental precipitation and genesis of sepiolite at earth-surface conditions, Am. Mineral., 53, 1645–1662, 1968.

1365 Xu, Y.-Y., Pierrot, D., and Cai, W.-J.: Ocean carbonate system computation for anoxic waters using an updated CO2SYS program, Mar. Chem., 195, 90–93, https://doi.org/10.1016/j.marchem.2017.07.002, 2017.

Yang, B., Leonard, J., and Langdon, C.: Seawater alkalinity enhancement with magnesium hydroxide and its implication for carbon dioxide removal, Mar. Chem., 104251, https://doi.org/10.1016/j.marchem.2023.104251, 2023.

Zeebe, R. E. and Wolf-Gladrow, D. (Eds.): Chapter 1 Equilibrium, in: Elsevier Oceanography Series, vol. 65, Elsevier, 1–84,
1370 https://doi.org/10.1016/S0422-9894(01)80002-7, 2001.

Zhu, Q., Aller, R. C., and Fan, Y.: Two-dimensional pH distributions and dynamics in bioturbated marine sediments, Geochim. Cosmochim. Acta, 70, 4933–4949, https://doi.org/10.1016/j.gca.2006.07.033, 2006.